Electronic Supplementary Material (ESI) for Inorganic Chemistry Frontiers.

Heptadentate chelates for ^{89}Zr-radiolabelling of monoclonal antibodies

Amaury Guillou[a], Ali Ouadi[b] and Jason P. Holland[a]*

[a] University of Zurich, Department of Chemistry, Winterthurerstrasse 190, CH-8057, Zurich, Switzerland

[b] Université de Strasbourg, CNRS, IPHC UMR 7178, F-67000, Strasbourg, France

*** Corresponding Author:**

Prof. Dr Jason P. Holland

Tel: +41.44.63.53.990

E-mail: jason.holland@chem.uzh.ch

Website: www.hollandlab.org

First Author:

Dr Amaury Guillou

E-mail: amaury.guillou@chem.uzh.ch

Table of content

Methods and Materials

General details

Unless otherwise stated, all chemicals were of reagent grade and were purchased from SigmaAldrich (St. Louis, MO), Merck (Darmstadt, Germany), Tokyo Chemical Industry (Eschborn, Germany), abcr (Karlsruhe, Germany). Water (>18.2 MΩ·cm at 25 ºC, Puranity TU 3 UV/UF, VWR International, Leuven, Belgium) was used without further purification. Solvents for reactions were of reagent grade, and where necessary, were dried over molecular sieves. Evaporation of the solvents was performed under reduced pressure by using a rotary evaporator (Rotavapor R-300, Büchi Labortechnik AG, Flawil, Switzerland).

^{1}H and ^{13}C{^{1}H} NMR spectra were measured in deuterated solvents on a Bruker AV-400 (^{1}H: 400 MHz, ^{13}C: 100.6 MHz) or a Bruker AV-500 (^{1}H: 500 MHz, ^{13}C: 125.8 MHz) spectrometer. Chemical shifts (δ) are expressed in parts per million (ppm) relative to the resonance of the residual solvent peaks. Coupling constants (*J*) are reported in Hz. Peak multiplicities are abbreviated as follows: s (singlet), d (doublet), dd (doublet of doublets), t (triplet), q (quartet), p (pentet), m (multiplet), and br s (broaden singlet).

High-resolution electrospray ionisation mass spectra (HR-ESI-MS) and elemental analyses were measured by the mass spectrometry / elemental analysis service at the Department of Chemistry, University of Zurich.

Column chromatography was performed by using Merck silica gel *60* (63 – 200 μm) with the eluents indicated in the experimental section. Standard thin-layer chromatography (TLC) for synthesis employed Merck TLC plates silica gel *60* on an aluminium base with the indicated solvent system. The spots on TLC were visualised either by UV/visible light (254 nm) or by staining with $KMnO_4$.

Analytical high-performance liquid chromatography (HPLC) experiments were performed using Hitachi Chromaster Ultra Rs systems fitted with a reverse phase VP 250/4 Nucleodur C18 HTec (4 mm ID x 250 mm, 5μm) column. This system was also connected to a radioactivity detector (FlowStar^{2} LB 514, Berthold Technologies, Zug, Switzerland) equipped with a 20 μL PET cell (MX-20-6, Berthold Technologies) for analysing radiochemical reactions. Proteins were analysed using the same HPLC system equipped with a size-exclusion column (Enrich

SEC 650 column: 24 mL volume, 10 mm ID x 300 mm, Bio-Rad Laboratories, Basel, Switzerland).

Photochemistry

Photochemical conjugation experiments were performed in transparent glass vials at the specified concentrations. Unless otherwise stated, photochemical reactions were typically stirred gently by adding a small magnetic stir bar to the reaction vial and employing a slow stirring rate (<1000 rpm) to avoid potential damage to the protein. Detailed procedures and reaction times are indicated in the experimental section. Ultra-violet irradiations were performed by using portable light-emitting diode (LED; 395 nm). The LED intensity was adjusted using a digital UV-LED controller (Opsytec Dr. Gröbel GmbH, Ettlingen, Germany), where 100% corresponded to a power of approximately 355 mW at 395 nm. LED intensity was measured by using a S470C Thermal Power Sensor Head Volume Absorber, 0.25 – 10.6 µm, 0.1 mW – 5W, Ø15 mm. The 395 nm LED had a maximum emission intensity at 389.9 nm (FWHM of 9.1 nm). The temperature of all photochemical conjugation reactions was typically 23 ± 2 ºC (ambient conditions).

Radioactivity and radioactive measurements

All instruments for measuring radioactivity were calibrated and maintained in accordance with previously reported routine quality control procedures.[1] $[^{89}Zr][Zr(C_2O_4)_4]^{4-}$(aq.) was obtained as a solution in ~1.0 M oxalic acid from PerkinElmer (Boston, MA, manufactured by the BV Cyclotron VU, Amsterdam, The Netherlands) and was used without further purification. Radioactive reactions were monitored by using instant thin-layer chromatography (radio-iTLC). Glass-fibre iTLC plates impregnated with silica-gel (iTLC-SG, Agilent Technologies) were developed in using aqueous mobile phases containing DTPA (50 mM, pH7.1) and were analysed on a radio-TLC detector (SCAN-RAM, LabLogic Systems Ltd, Sheffield, United Kingdom). Radiochemical conversion (RCC) was determined by integrating the data obtained by the radio-TLC plate reader and determining both the percentage of radiolabelled product (R_f = 0.0) and 'free' ^{89}Zr (R_f = 1.0; present in the analyses as $[^{89}Zr][Zr(DTPA)]^-$). Integration and data analysis were performed by using the software Laura version 5.0.4.29 (LabLogic). Appropriate background and decay corrections were applied as necessary. Radiochemical purities (RCPs) of labelled protein samples were determined by size-exclusion chromatography (SEC) using two different columns and techniques. The first technique used an automated size-exclusion column (Bio-Rad Laboratories, ENrich SEC 70, 10 ± 2 µm, 10 mm ID x 300 mm)

connected to a Rigol HPLC system (Contrec AG, Dietikon, Switzerland) equipped with a UV/visible detector (absorption measured at 220, 254 and 280 nm) as well as a radioactivity detector (FlowStar^2 LB 514, Berthold Technologies, Zug, Switzerland). Isocratic elution with phosphate buffered saline (PBS, pH7.4) was used. The second method used a manual procedure involving size-exclusion column chromatography and a PD-10 desalting column (Sephadex G-25 resin, 85-260 µm, 14.5 mm ID × 50 mm, >30 kDa, GE Healthcare). For analytical procedures, PD-10 columns were eluted with PBS. A total of 40 × 200 µL fractions were collected up to a final elution volume of 8 mL. Note that the loading/dead-volume of the PD-10 columns is precisely 2.50 mL which was discarded prior to aliquot collection. For quantification of radioactivity, each fraction was measured on a gamma counter (HIDEX Automatic Gamma Counter, Hidex AMG, Turku, Finland) using an energy window between 480 – 558 keV for ^{89}Zr (511 keV emission) and a counting time of 30 s. Appropriate background and decay corrections were applied throughout. PD-10 SEC columns were also used for preparative purification and reformulation of radiolabelled products (in sterile PBS; pH7.4) by collecting a fraction of the eluate corresponding to the high molecular weight protein (>30 kDa fraction eluted in the range 0.0 mL to 1.6 mL as indicated for each experiment).

^{89}Zr-radioactive stocks

Stock solutions of $[^{89}Zr][Zr(C_2O_4)_4]^{4-}$ were prepared on several occasions using the same procedure. As an example, a stock solution of $[^{89}Zr][Zr(C_2O_4)_4]^{4-}$ was prepared by adding ^{89}Zr radioactivity from the source (172.2 MBq, 150 µL in ~1.0 M aqueous oxalic acid; PerkinElmer) to an Eppendorf tube. The solution was neutralised by the addition of aliquots of Na_2CO_3(aq.) (1.0 M stock solution, total volume of 180 µL added, final pH ~7.5 – 7.7, final volume ~345 µL, final activity = 169.7 MBq). Caution: Acid neutralisation with Na_2CO_3 releases CO_2(g) and care should be taken to ensure that no radioactivity escapes the microcentrifuge tube. After CO_2 evolution ceased, multiple reactions were performed by using the same stock solutions.

Cell culture

For cell binding assays, the human gastric cancer cell line MKN45 was used. Cells were cultured at 37 °C in a humidified 5% CO_2 atmosphere. MKN45 cells were cultured in RPMI. The media was supplemented with fetal bovine serum (FBS, 10% (v/v), ThermoFisher Scientific) and penicillin/streptomycin (P/S, 1% (v/v) of penicillin 10000 U/mL and streptomycin 10 mg/mL). Cells were grown by serial passage and were harvested using trypsin-

EDTA solution (0.25%). Cells were pelleted (100 g, 5 min) and resuspended in media before sequential passaging.

Animals and xenograft models

All experiments involving mice were conducted in accordance with the ARRIVE 2.0 guidelines on experimental good practice and an animal experimentation licence approved by the Zurich Canton Veterinary Office, Switzerland (Jason P. Holland).[2] Female athymic nude mice (Crl:NU(NCr)-*Foxn1*^{nu}, 20 – 25 g, 4 – 8 weeks old) were obtained from Charles River Laboratories Inc. (Freiburg im Breisgau, Germany), and were allowed to acclimatise at the University of Zurich Laboratory of Animal Science vivarium for at least 1 week prior to implanting tumour cells. Mice were provided with food and water *ad libitum*. Tumours were induced on the right shoulder or flank by sub-cutaneous (s.c.) injection of approx. 2.5×10^6 cells. The cells were injected in a 200 µL suspension of a 1:1 v/v mixture of PBS and reconstituted basement membrane (Corning® Matrigel® Basement Membrane Matrix, obtained from VWR International).[3] Tumours developed after a period of between 7 – 14 days. Tumour volume (V / mm^3) was estimated by external Vernier calliper measurements of the longest axis, a / mm, and the axis perpendicular to the longest axis, b / mm. The tumours were assumed to be spheroidal and the volume was calculated in accordance with Equation S1.

$$V = \frac{4\pi}{3} \cdot \left(\frac{a}{2}\right)^2 \cdot \left(\frac{b}{2}\right) \qquad \text{(Equation S1)}$$

Small-animal PET imaging

All mice injected with cancer cells developed tumours and the average volume of the MKN45 tumours was 172 ± 168 mm^3 (n = 6 mice). Mice were randomised before the study. The tail of each mouse was warmed gently by using a warm water bath immediately before administering [^{89}Zr]ZrDFO-Gly-Glu-Gly-PEG$_3$-azepin-onartuzumab (normal group n = 3 mice / group, where each dose contained activity = 0.195–0.204 MBq, 59–72 µg of protein, in 200 µL sterile PBS) *via* intravenous (i.v.) tail-vein injection (t = 0 h). Competitive inhibition studies were also performed to investigate the specificity and biological activity of the radiotracer *in vivo* (blocking group: n = 3 mice / group, where each dose contained activity = 0.203–0.210 MBq, in 200 µL sterile PBS). To the blocking formulation, an aliquot of MetMAb^{TM} stock protein (fully formulated; 60 mg/mL, 3 µL, 4.98 mg of protein) was added to reduce the molar activity (total = 823–834 mg of protein / mouse).

PET imaging experiments were conducted on a Genesis G4 PET/X-ray scanner (Sofie Biosciences, Culver City, CA).[4] Approximately 5 minutes prior to recording each PET image, mice were anesthetised by inhalation of between ~4% isoflurane (Attane^{TM}, Piramal Enterprises Ltd, India, supplied by Provet AG, Lyssach, Switzerland)/oxygen gas mixture and placed on the scanner bed in the prone position. PET images were recorded at various time-points between 0 h and 72 h post-administration of the radiotracer. During image acquisition, the respiration rate of the animal was monitored *via* live video feed and anaesthesia was maintained by an experience animal experimenter by controlling the isoflurane dose between 1.5 – 2.0%. List-mode data were acquired for 10 min. using a γ-ray energy window of 150–650 keV, and a coincidence timing window of 20 ns. Images were reconstructed by iterative ordered subset maximum expectation (OSEM; 60 iterations) protocols. The reported reconstructed spatial resolution is 2.4 μL at the centre of the field-of-view (FOV). Image data were normalised to correct for non-uniformity of response of the PET, attenuation, random events, dead-time count losses, positron branching ratio, and physical decay to the time of injection, but no scatter or partial-volume averaging correction was applied. An empirically determined system calibration factor (in units of [Bq/voxel]/[MBq/g] or [Bq/cm^3]/[MBq/g]) for mice was used to convert voxel count rates to activity concentrations. The resulting image data were normalised to the administered activity to parameterise images in terms of %ID cm^{-3} (equivalent to units of %ID/g assuming a tissue density of unity). Images were analysed by using VivoQuant^{TM} 3.5 patch 2 software (InviCRO, Boston, MA). For image quantification and measurements of time-activity curves (TACs), 3-dimensional volumes-of-interest (VOIs) were drawn manually to determine the maximum and mean accumulation of radioactivity (in units of %ID cm^{-3} and decay corrected to the time of injection) in various tissues. Where appropriate, data were also converted into mean standardised uptake values (SUV_{mean}).

Biodistribution studies

Biodistribution studies were conducted after the final imaging time point to evaluate the radiotracer uptake in tumour-bearing mice. Animals were anaesthetised individually by isoflurane and euthanised by isoflurane asphyxiation followed by terminal exsanguination. A total of 14 tissues (including the tumour) were removed, rinsed in water, dried in air for approx. 2 min., weighed and counted on a calibrated gamma counter for accumulation of activity. The mass of radiotracer formulation injected into each animal was measured and used to determine the total number of counts per minute (cpm) injected into each mouse by comparison to a

standard syringe of known activity and mass. Count data were background- and decay-corrected, and the tissue uptake for each sample (determined in units of percentage injected dose per gram [%ID g^{-1}]) was calculated by normalisation to the total amount of activity injected for each individual animal.

Effective half-life, $t_{1/2}$(eff)

The effective half-live $t_{1/2}$(eff) of [^{89}Zr]ZrDFO-**2**-onartuzumab was measured in the same athymic nude mice used for small-animal PET imaging and end time point biodistribution. Total internal radioactivity was measured as a function of time by using a dose calibrator.

Statistical analysis

Where appropriate, data were analysed by the unpaired, two-tailed Student's *t*-test. Differences at the 95% confidence level (*P*-value <0.05) were statistically significant. Data analysis was performed using Microsoft Excel for MAC (version 16.16.10) and GraphPad Prism 7 for MAC OS X (version 7.0e)

Computational details

All calculations were conducted using density functional theory (DFT) as implemented in the Gaussian16 Revision A.03 suite of *ab initio* quantum chemistry programs.[5] Normal self-consistent field (SCF) and geometry convergence criteria were employed throughout. All structures were optimised in solution phase using a polarisable continuum model (PCM) without symmetry constraints. Solvated phase calculations were implemented by using the SCRF keyword with default parameters and selecting water as the solvent (dielectric constant, $\varepsilon = 78.3553$).[6] Harmonic frequency analysis based on analytical second derivative was used to characterise the optimised structures as local minima or first order saddle points (transition states) on the potential energy surface. Calculations were performed by using the unrestricted B3LYP[7–9] exchange-correlation functionals and the double-ζ DGDZVP[10,11] basis set. The choice of solvation model reflects the aqueous phase conditions employed in the ^{89}Zr-radiolabelling of molecules bearing the DFO chelate. Optimised structures and molecular orbitals were analysed by using Chemcraft (version 1.8, build 536b, www.chemcraftprog.com).

Synthesis of the metal binding chelates

General procedure A.

In a plastic syringe, 2-chlorotritylchloride resin (100-200 mesh, 1.71 mmol/g) was swelled in CH_2Cl_2 (3 × 1 min). The first Fmoc protected amino acid (Fmoc-AA-OH, 2 eq.) was solubilized in CH_2Cl_2 with DIPEA (3 eq.) then the mixture was incorporated in the syringe as a coupling system. The syringe was shaken for 10 min before the addition of DIPEA (7eq.) and the shaking was continued for 45 min. Methanol (500 µL) was added to cap unreacted functional groups on the resin and the resulting mixture was shaken for 10 min. The resin was filtered and washed with CH_2Cl_2 (×3), DMF (×3) and CH_2Cl_2 (×3). The Fmoc group was deprotected using a solution of 20% of piperidine in DMF for 5 min three times. The resin was washed with CH_2Cl_2 (×3), DMF (×3) and CH_2Cl_2 (×3) and dried. Elongation of the peptidic chain was performed by adding Fmoc-AA-OH (3 eq.) and HBTU (2.9 eq.), DIPEA (6 eq.) in DMF (5 mL) to the resin. The resulting mixture was stirred for 90 min. After completion, the resin was washed with DMF (×3) and CH_2Cl_2 (×3). Deprotection of Fmoc was made as described and the coupling cycles were repeated with the appropriate amino acids to provide a tripeptide. Then, ArN_3-PEG_3-NH-succ[33] (1.44 eq), HBTU (2.9 eq) and DIPEA (6 eq) were added to the syringe and DMF (5 mL). The syringe was shaken for 90 min. After completion, the resin was washed with CH_2Cl_2 (×3), DMF (×3) and CH_2Cl_2 (×3). The crude compounds were cleaved from the resin using a 1% TFA solution in CH_2Cl_2. The solvent was removed in vaccuo to obtain the crude peptides. Compounds **6a-c** were purified by flash chromatography on C-18 using MeOH (0.1% TFA)/H_2O (0.1% TFA) with the gradient 0% to 100% MeOH (0.1% TFA).

Compound 6a was obtained following general procedure A starting from Fmoc-Gly-OH (461 mg, 1.55 mmol) as a yellow oil (249 mg, 54%).**^{1}H NMR** (400 MHz, MeOD, 298 K) δ (ppm) 7.92 – 7.79 (d, *J* = 8.1 Hz, 2H, CH_{Ar}), 7.19 – 7.05 (d, *J* = 8.1 Hz, 2H, CH_{Ar}), 4.45 (dd, *J* = 9.2, 4.9 Hz, 1H, CH), 3.92 (d, *J* = 5.5 Hz, 2H, CH_2), 3.87 (s, 2H, CH_2), 3.68 – 3.50 (m, 10H, CH_2 PEG), 3.47 (td, *J* = 6.5, 2.1 Hz, 4H, CH_2), 3.23 (t, *J* = 6.8 Hz, 2H, CH_2), 2.62 – 2.44 (m, 4H, CH_2), 2.42 – 2.28 (m, 2H, CH_2), 2.16 (dtd, *J* = 16.0, 7.5, 5.1 Hz, 1H CH), 2.01 – 1.80 (m, 3H, CH_2), 1.72 (p, *J* = 6.5 Hz, 2H, CH_2), 1.43 (s, 9H, CH_3). **^{13}C{^{1}H} NMR** (101 MHz, MeOD, 298 K) δ (ppm) 175.8 (C=O), 174.5 (C=O), 173.6 (C=O), 172.4 (C=O), 171.6 (C=O), 168.9 (C=O), 144.6 (C_{qt}), 132.2 (C_{qt}), 130.1 (CH_{Ar}), 119.9 (CH_{Ar}), 81.7 (C_{qt}), 71.4, 71.1, 70.2, 69.8 (CH_2 PEG), 52.8 (CH), 44.1 (CH_2), 43.3 (CH_2), 38.7 (CH_2), 37.8 (CH_2), 32.5 (CH_2), 32.0 (CH_2), 31.9

(CH_2), 30.3 (CH_2), 28.3 (CH_3), 27.8 (CH_2). **ESI-HR-MS** *m/z* calcd. for $[C_{34}H_{52}N_8O_{12}+H]^+$ 765.37775, found 765.37817.

Compound 6b was obtained following general procedure A starting from Fmoc-Gly-OH (508 mg, 1.71 mmol) as a yellow oil (354 mg, 52%).**^{1}H NMR** (400 MHz, DMSO, 298 K) δ (ppm) 8.43 (t, *J* = 5.6 Hz, 1H, N*H*), 8.19 (t, *J* = 5.8 Hz, 1H, N*H*), 8.13 (t, *J* = 5.9 Hz, 1H, N*H*), 8.04 (d, *J* = 8.1 Hz, 1H, N*H*), 7.92 – 7.81 (m, 3H, CH_{Ar} + N*H*), 7.20 – 7.12 (d, *J* = 8.1 Hz, 2H, CH_{Ar}), 4.29 (td, *J* = 8.4, 5.1 Hz, 1H, CH), 3.82 – 3.64 (m, 4H, CH_2), 3.55 – 3.40 (m, 10H, CH_2 PEG), 3.36 (t, *J* = 6.4 Hz, 3H, CH_2), 3.30 (q, *J* = 6.6 Hz, 3H, CH_2), 3.06 (q, *J* = 6.6 Hz, 2H, CH_2), 2.34 (s, 4H, CH_2), 2.28 – 2.17 (m, 2H, CH_2), 1.93 (qd, *J* = 8.2, 3.3 Hz, 2H, CH_2), 1.74 (p, *J* = 6.4 Hz, 3H, CH_2), 1.60 (q, *J* = 6.7 Hz, 2H, CH_2), 1.37 (s, 9H, CH_3). **^{13}C{^{1}H} NMR** (101 MHz, DMSO, 298 K) δ (ppm) 172.5 (C=O), 171.9 (C=O), 171.7 (C=O), 171.6 (C=O), 171.2 (C=O), 169.3 (C=O), 165.4 (C=O), 142.3 (C_{qt}), 131.3 (C_{qt}), 129.2 (CH_{Ar}), 118,9 (CH_{Ar}) 79.7 (C_{qt}), 69.9, 69.7, 68.5, 68.2 (CH_2 PEG), 51.8 (CH), 42.4 (CH_2), 40.8 (CH_2), 36.9 (CH_2), 36.0 (CH_2), 31.3 (CH_2), 30.9 (CH_2), 29.5 (CH_2), 27.8 (CH_3), 27.3 (CH_2). **ESI-HR-MS** *m/z* calcd. for $[C_{34}H_{52}N_8O_{12}+H]^+$ 765.37775, found 765.37843.

Compound 6c was obtained following general procedure A starting from Fmoc-Glu(O^{t}Bu)-OH (728 mg, 1.71 mmol) as a yellow oil (186 mg, 28%).**^{1}H NMR** (400 MHz, MeOD, 298 K) δ (ppm) 7.92 – 7.79 (d, *J* = 8.1 Hz, 2H, CH_{Ar}), 7.19 – 7.05 (d, *J* = 8.1 Hz, 2H, CH_{Ar}), 4.45 (dd, *J* = 9.2, 4.9 Hz, 1H, CH), 3.92 (d, *J* = 5.5 Hz, 2H, CH_2), 3.87 (s, 2H, CH_2), 3.68 – 3.50 (m, 10H, CH_2 PEG), 3.47 (td, *J* = 6.5, 2.1 Hz, 4H, CH_2), 3.23 (t, *J* = 6.8 Hz, 2H, CH_2), 2.62 – 2.44 (m, 4H, CH_2), 2.42 – 2.28 (m, 2H, CH_2), 2.16 (dtd, *J* = 16.0, 7.5, 5.1 Hz, 2H, CH_2), 2.01 – 1.80 (m, 3H, CH_2), 1.72 (p, *J* = 6.5 Hz, 2H, CH_2), 1.43 (s, 9H, CH_3). **^{13}C{^{1}H} NMR** (101 MHz, MeOD, 298 K) δ (ppm) 175.8 (C=O), 174.7 (C=O), 173.6 (C=O), 172.4 (C=O), 171.6 (C=O), 168.8 (C=O), 144.6 (C_{qt}), 132.2 (C_{qt}), 130.1 (CH_{Ar}), 119.9 (CH_{Ar}), 81.7 (C_{qt}), 71.4 (C_{qt}), 71.1, 70.2, 69.8 (CH_2 PEG), 52.8 (CH), 44.1 (CH_2), 43.3 (CH_2), 38.7 (CH_2), 37.8 (CH_2), 32.5 (CH_2), 32.0 (CH_2), 31.9 (CH_2), 30.3 (CH_2), 28.3 (CH_2), 27.8 (CH_3). **ESI-HR-MS** *m/z* calcd. for $[C_{34}H_{52}N_8O_{12}+H]^+$ 765.37775, found 765.37818.

General procedure B.

Compounds **6a-c** and HATU (1.5 eq) were dissolved in DMF and HATU (1.5 eq.) and DIPEA (4 eq.) was added. The mixture was stirred for 40 min and then DFO-mesylate (1.2 eq.) was added. The resulting solution was left to stir overnight at rt. After completion of the reaction,

the mixture was dried in vacuo and purified by flash chromatography with C-18 column using MeOH (0.1% TFA) / H_2O (0.1% TFA) with the gradient 0% to 100% MeOH (0.1% TFA) to give the desired compounds as off-white solids.

Compound **5a** was obtained starting from **6a** (216 mg, 0.28 mmol) following general procedure B as a white solid (244 mg, 66%).
^{1}H NMR (500 MHz, DMSO) δ (ppm) 8.44 (t, *J* = 5.6 Hz, 1H, N*H*), 8.22 (t, *J* = 5.6 Hz, 1H, N*H*), 8.13 (d, *J* = 7.3 Hz, 1H, N-O*H*), 8.00 (d, *J* = 6.0 Hz, 1H, N-O*H*), 7.90 – 7.87 (m, 2H, CH_{Ar}), 7.83 (t, *J* = 5.7 Hz, 1H, N*H*), 7.77 (t, *J* = 5.6 Hz, 1H, N*H*), 7.67 (t, *J* = 5.7 Hz, 1H, N*H*), 7.24 – 7.12 (m, 2H, CH_{Ar}), 4.19 (td, *J* = 8.1, 5.3 Hz, 1H, CH), 3.77 – 3.60 (m, 3H, CH_2), 3.57 – 3.41 (m, 13H, CH_2 PEG), 3.37 (t, *J* = 6.4 Hz, 2H, CH_2), 3.30 (q, *J* = 6.6 Hz, 2H, CH_2), 3.10 – 2.95 (m, 6H, CH_2), 2.57 (t, *J* = 7.4 Hz, 2H, CH_2), 2.43 – 2.17 (m, 8H, CH_2), 1.96 (s, 3H, CH_3), 1.74 (p, *J* = 6.6 Hz, 3H, CH_2), 1.59 (p, *J* = 6.7 Hz, 2H, CH_2), 1.50 (q, *J* = 7.6 Hz, 4H, CH_2), 1.38 (s, 12H, CH_3 + CH_2), 1.30 – 1.11 (m, 5H, CH_2). **^{13}C{^{1}H} NMR** (126 MHz, DMSO) δ (ppm) 172.1 (C=O), 172.0 (C=O), 171.9 (C=O), 171.7 (C=O), 171.6 (C=O), 171.4 (C=O), 171.3 (C=O), 170.2 (C=O), 169.3 (C=O), 169.0 (C=O), 168.4 (C=O), 165.2 (C=O), 162.3 (C=O), 142.1 (C_{qt}), 131.2 (C_{qt}), 129.1 (CH_{Ar}), 118.9 (CH_{Ar}), 79.7 (Cqt), 69.8, 69.8, 69.6, 69.5, 68.3, 68.1 (CH_2 PEG), 52.1 (CH), 47.1 (CH_2), 46.8 (CH_2), 38.5 (CH_2), 38.4 (CH_2), 36.7 (CH_2), 35.8 (CH_2), 35.8 (CH_2), 31.3 (CH_2), 30.7 (CH_2), 30.6 (CH_2), 29.9 (CH_2), 29.4 (CH_2), 29.3 (CH_2), 28.8 (CH_2), (CH_2), 28.7 (CH_2), 27.8 (CH_3), 27.6 (CH_2), 26.9 (CH_2), 26.1 (CH_2), 23.5 (CH_2), 23.4 (CH_2), 20.4 (CH_3). **ESI-HR-MS** *m/z* calcd. for $[C_{59}H_{96}N_{14}O_{19}+2H]^{2+}$ 654.36391, found 654.36315.

Compound **5b** was obtained starting from **6b** (164 mg, 0.21 mmol) following general procedure B as a white solid (146 mg, 53%). **^{1}H NMR** (500 MHz, DMSO, 298 K) δ (ppm) 9.71 – 9.40 (m, 2H, N-O*H*), 8.37 (t, *J* = 5.6 Hz, 1H, N*H*), 8.20 – 7.92 (m, 2H, N*H*), 7.79 (dd, *J* = 14.5, 7.1 Hz, 2H, CH_{Ar}), 7.70 (t, *J* = 5.8 Hz, 1H, N*H*), 7.56 (t, *J* = 5.6 Hz, 1H, N*H*), 7.11 (d, *J* = 8.1 Hz, 2H, CH_{Ar}), 4.24 – 4.01 (m, 1H, CH), 3.88 – 3.16 (m, 20H, CH_2 PEG), 3.16 – 2.79 (m, 6H, CH_2), 2.50 (t, *J* = 7.4 Hz, 2H, CH_2), 2.39 – 2.05 (m, 7H, CH_2), 1.89 (s, 3H, CH_3), 1.69 (dt, *J* = 13.5, 7.1 Hz, 2H, CH_2), 1.52 (p, *J* = 6.7 Hz, 2H, CH_2), 1.48 – 1.37 (m, 3H, CH_2), 1.31 (s, 9H, CH_3), 1.14 (q, *J* = 7.9 Hz, 4H, CH_2). **^{13}C{^{1}H} NMR** (126 MHz, DMSO, 298 K) δ (ppm) 172.3 (C=O), 172.0 (C=O), 171.7 (C=O), 171.4 (C=O), 171.3 (C=O), 170.1 (C=O), 169.6 (C=O), 168.3 (C=O), 165.2 (C=O), 142.1 (C_{qt}), 131.2 (C_{qt}), 129.0 (CH_{Ar}), 118.9 (CH_{Ar}), 79.7 (C_{qt}), 69.8, 69.6, 68.8, 68.1 (CH_2 PEG), 52.2 (CH), 46.9 (CH_2), 42.2 (CH_2), 42.0 (CH_2), 38.4 (CH_2), 36.7 (CH_2),

35.8 (CH_2), 31.2 (CH_2), 30.7 (CH_2), 29.9 (CH_2), 29.3 (CH_2), 28.8 (CH_2), 27.7 (CH_3), 27.6 (CH_2), 26.8 (CH_2), 26.0 (CH_2), 23.5 (CH_2), 20.4 (CH_3). **ESI-HR-MS** *m/z* calcd. for $[C_{59}H_{96}N_{14}O_{19}+2H]^{2+}$ 654.36391, found 654.36315.

Compound **5c** was obtained starting from **6c** (167 mg, 0.21 mmol) following general procedure B a white solid (228 mg, 80%).

^{1}H NMR (400 MHz, DMSO, 298 K) δ (ppm) 8.44 (t, *J* = 5.6 Hz, 1H, N-O*H*), 8.28 (t, *J* = 5.8 Hz, 1H, N-O*H*), 8.19 (t, *J* = 5.9 Hz, 1H, N-O*H*), 7.90 – 7.83 (m, 4H, CH_{Ar} + N*H*), 7.79 (d, *J* = 5.8 Hz, 2H, CH_{Ar}), 7.77 – 7.72 (m, 1H, CH), 7.20 – 7.12 (m, 2H, CH_2), 4.18 (dt, *J* = 8.3, 4.1 Hz, 2H, CH_2), 3.70 (dd, *J* = 15.3, 5.6 Hz, 4H, CH_2), 3.56 – 3.40 (m, 17H, CH_2 PEG), 3.36 (t, *J* = 6.3 Hz, 2H, CH_2), 3.30 (q, *J* = 6.7 Hz, 2H, CH_2), 3.02 (dp, *J* = 18.5, 6.3 Hz, 10H, CH_2), 2.58 (d, *J* = 6.9 Hz, 4H, CH_2), 2.35 (dd, *J* = 6.6, 4.2 Hz, 4H, CH_2), 2.28 (d, *J* = 7.4 Hz, 4H, CH_2), 2.22 – 2.12 (m, 2H, CH_2), 1.96 (s, 3H, CH_3), 1.73 (dt, *J* = 11.3, 5.7 Hz, 3H, CH_2), 1.59 (t, *J* = 6.7 Hz, 2H, CH_2), 1.49 (t, *J* = 7.8 Hz, 5H, CH_2), 1.36 (s, 15H, CH_2), 1.29 – 1.17 (m, 6H, CH_2).

^{13}C{^{1}H} NMR (101 MHz, DMSO, 298 K) δ (ppm) 172.7 (C=O), 172.2 (C=O), 171.8 (C=O), 171.7 (C=O), 171.7 (C=O), 170.9 (C=O), 170.4 (C=O), 170.0 (C=O), 169.0 (C=O), 165.5 (C=O), 162.5 (C=O), 142.3 (C_{qt}), 131.3 (C_{qt}), 129.2 (CH_{Ar}), 119.0 (CH_{Ar}), 79.9, 70.0, 69.9, 69.7, 69.7, 68.5, 68.2 (CH_2 PEG), 52.1 (CH), 48.7 (CH_2), 47.3 (CH_2), 47.0 (CH_2), 42.6 (CH_2), 42.3 (CH_2), 38.7 (CH_2), 38.6 (CH_2), 36.9 (CH_2), 36.0 (CH_2), 35.9 (CH_2), 31.5 (CH_2), 30.9 (CH_2), 30.9 (CH_2), 30.7 (CH_2), 30.1 (CH_2), 29.5 (CH_2), 29.4 (CH_2), 28.9 (CH_2), 28.8 (CH_2), 27.8 (CH_3), 27.7 (CH_2), 27.4 (CH_2), 26.2 (CH_2), 26.1 (CH_2), 23.6 (CH_2), 23.6 (CH_2), 20.4 (CH_3). **ESI-HR-MS** *m/z* calcd. for $[C_{59}H_{96}N_{14}O_{19}+2H]^{2+}$ 654.36391, found 654.36366.

General procedure C.

Compounds **5a-c** were dissolved in a solution of 1mL TFA in water (1/1 v/v) and the mixture was stirred at rt for 2 h. After that, the resulting mixture was poored in Et_2O (50 mL) and let to sit at -20°C for 24 h. The resulting precipitates were filtered, washed with Et_2O (3 × 5 mL), suspended in 3 mL of a water/acetonitrile (1/1 v/v) mixture and freezed dried to obtain the resulting final compounds as off-white to yellow solids.

DFO-Gly-Gly-Glu-PEG_3-ArN_3 (**1**) was obtained starting from **5a** (40 mg, 0.03 mmol) following general procedure C as a white solid (29 mg, 76%).

^{1}H NMR (500 MHz, DMSO) δ (ppm) 9.73 – 9.54 (m, 2H, N-O*H*), 8.44 (t, *J* = 5.6 Hz, 1H, N*H*), 8.22 (t, *J* = 5.7 Hz, 1H, N*H*), 8.13 (d, *J* = 7.5 Hz, 1H, N*H*), 8.02 (t, *J* = 6.0 Hz, 1H, N*H*), 7.88

(d, *J* = 8.2 Hz, 2H, CH_{Ar}), 7.83 (t, *J* = 5.6 Hz, 1H, N*H*), 7.77 (t, *J* = 5.7 Hz, 2H, N*H*), 7.68 (t, *J* = 5.8 Hz, 1H, N*H*), 7.19 (d, *J* = 8.2 Hz, 2H, CH_{Ar}), 4.19 (td, *J* = 8.1, 5.3 Hz, 1H, CH), 3.75 – 3.60 (m, 4H, CH_2), 3.57 – 3.42 (m, 15H, CH_2 PEG), 3.37 (t, *J* = 6.4 Hz, 3H, CH_2), 3.30 (q, *J* = 6.6 Hz, 3H, CH_2), 3.14 – 2.95 (m, 7H, CH_2), 2.57 (t, *J* = 7.5 Hz, 3H, CH_2), 2.45 – 2.21 (m, 9H, CH_2), 1.96 (s, 3H, CH_3), 1.74 (p, *J* = 6.9 Hz, 3H, CH_2), 1.59 (p, *J* = 6.7 Hz, 3H, CH_2), 1.49 (h, *J* = 6.3 Hz, 4H, CH_2), 1.39 (h, *J* = 7.8 Hz, 5H, CH_2), 1.21 (q, *J* = 7.7 Hz, 5H, CH_2). **^{13}C{^{1}H} NMR** (126 MHz, DMSO) δ (ppm) 174.0 (C=O), 172.1 (C=O), 172.1 (C=O), 172.0 (C=O), 171.7 (C=O), 171.4 (C=O), 171.3 (C=O), 170.1 (C=O), 169.0 (C=O), 168.4 (C=O), 165.2 (C=O), 142.1 (C_{qt}), 131.2 (C_{qt}), 129.0 (CH_{Ar}), 118.7 (CH_{Ar}), 69.8, 69.8, 69.6, 69.5, 68.3, 68.1 (CH_2 PEG), 52.2 (CH), 47.1 (CH_2), 46.8 (CH_2), 42.3 (CH_2), 42.0 (CH_2), 38.5 (CH_2), 38.4 (CH_2), 36.7 (CH_2), 35.8 (CH_2), 30.7 (CH_2), 30.7 (CH_2), 30.1 (CH_2), 29.9 (CH_2), 29.4 (CH_2), 29.3 (CH_2), 28.8 (CH_2), 28.7 (CH_2), 27.6 (CH_2), 26.9 (CH_2), 26.0 (CH_2), 23.5 (CH_2), 23.5 (CH_2), 20.4 (CH_3). **ESI-HR-MS** (negative mode) *m/z* calcd. for $[C_{55}H_{90}N_{14}O_{19}\text{-}H]^-$ 1250.65067, found 1250.64376.

DFO-Gly-Glu-Gly-PEG_3-ArN_3 (**2**) was obtained starting from **5b** (28 mg, 0.02 mmol) following general procedure C as a white solid (24 mg, 90%).
^{1}H NMR (500 MHz, DMSO) δ (ppm) 9.80 – 9.60 (m, 2H, N-O*H*), 8.46 (t, *J* = 5.6 Hz, 1H, N*H*), 8.21 (t, *J* = 6.2 Hz, 1H, N*H*), 8.09 (t, *J* = 6.3 Hz, 1H, N*H*), 7.88 (d, *J* = 8.3 Hz, 3H, CH_{Ar} + N*H*), 7.79 (t, *J* = 5.6 Hz, 2H, N*H*), 7.64 (t, *J* = 5.7 Hz, 1H, N*H*), 7.18 (d, *J* = 8.2 Hz, 2H, CH_{Ar}), 4.24 – 4.13 (m, 1H, CH), 3.75 – 3.59 (m, 4H, CH_2), 3.57 – 3.25 (m, 27H, CH_2 PEG + CH_2), 3.12 – 2.96 (m, 6H, CH_2), 2.57 (t, *J* = 7.6 Hz, 3H, CH_2), 2.39 – 2.20 (m, 8H, CH_2), 1.96 (s, 3H, CH_3), 1.76 (dp, *J* = 13.4, 6.9 Hz, 3H, CH_2), 1.59 (p, *J* = 6.6 Hz, 3H, CH_2), 1.49 (p, *J* = 7.5 Hz, 3H, CH_2), 1.38 (m, 4H, CH_2), 1.21 (m, 4H, CH_2). **^{13}C{^{1}H} NMR** (126 MHz, DMSO) δ (ppm) 174.0 (C=O), 172.3 (C=O), 172.0, (C=O) 171.5 (C=O), 171.4 (C=O), 171.4 (C=O), 171.4 (C=O), 170.2 (C=O), 170.1 (C=O), 169.6 (C=O), 168.4 (C=O), 165.23 (C=O), 142.2 (C_{qt}), 131.2 (C_{qt}), 129.1 (CH_{Ar}), 118.9 (CH_{Ar}), 69.8, 69.8, 69.6, 69.5, 68.3, 68.1 (CH_2 PEG), 52.4 (CH), 51.7 (CH_2), 47.1 (CH_2), 46.8(CH_2), 42.3 (CH_2) , 42.1 (CH_2), 36.7 (CH_2), 35.8 (CH_2), 30.8 (CH_2), 30.6 (CH_2), 30.1 (CH_2), 29.7 (CH_2), 29.4, 29.3 (CH_2), 28.8 (CH_2), 28.7 (CH_2), 27.6 (CH_2), 26.8 (CH_2), 26.1 (CH_2), 23.5 (CH_2), 23.5 (CH_2), 20.4 (CH_3). **ESI-HR-MS** (negative mode) *m/z* calcd. for $[C_{55}H_{90}N_{14}O_{19}\text{-}H]^-$ 1250.65067, found 1250.64643. **EA** calcd.

DFO-Glu-Gly-Gly-PEG_3-ArN_3 (**3**) was obtained starting from **5c** (25 mg, 0.02 mmol) following general procedure C as a white solid (21 mg, 88%).

^{1}H NMR (500 MHz, DMSO) δ (ppm) 9.70 – 9.57 (m, 2H, N-O*H*), 8.45 (t, *J* = 5.6 Hz, 1H, N*H*), 8.26 (q, *J* = 4.5 Hz, 1H, N*H*), 8.16 (t, *J* = 5.7 Hz, 1H, N*H*), 7.93 – 7.82 (m, 3H, CH_{Ar} + N*H*), 7.82 – 7.74 (m, 2H, N*H*), 7.19 (d, *J* = 8.5 Hz, 2H, CH_{Ar}), 4.19 (td, *J* = 8.5, 5.0 Hz, 1H, CH), 3.75 – 3.64 (m, 3H, CH_2), 3.56 – 3.25 (m, 26H, CH_2 PEG + CH_2), 3.16 – 2.91 (m, 7H, CH_2), 2.57 (t, *J* = 7.4 Hz, 2H, CH_2), 2.41 – 2.14 (m, 8H, CH_2), 1.96 (s, 3H, CH_3), 1.74 (m, 3H, CH_2), 1.59 (p, *J* = 6.8 Hz, 2H, CH_2), 1.49 (p, *J* = 7.3 Hz, 3H, CH_2), 1.38 (m, 4H, CH_2), 1.33 – 1.11 (m, 5H, CH_2). **^{13}C{^{1}H} NMR** (126 MHz, DMSO) δ (ppm) 173.9 (C=O), 172.4 (C=O), 172.0 (C=O), 171.4 (C=O), 171.3 (C=O), 170.7 (C=O), 170.1 (C=O), 169.7 (C=O), 168.7 (C=O), 165.2 (C=O), 142.1 (C_{qt}), 131.2 (C_{qt}), 129.0 (CH_{Ar}), 118.9 (CH_{Ar}), 72.5, 69.8, 69.8, 69.6, 69.5, 68.3, 68.0 (CH_2 PEG), 63.1 (CH_2), 51.9 (CH), 50.2, 47.1 (CH_2), 46.8 (CH_2), 42.3 (CH_2), 42.1 (CH_2), 38.5 (CH_2), 38.4 (CH_2), 36.7 (CH_2), 35.8 (CH_2), 30.7 (CH_2), 30.6 (CH_2), 30.1 (CH_2), 29.9 (CH_2), 29.3 (CH_2), 29.3 (CH_2), 28.8 (CH_2), 28.7 (CH_2), 27.6 (CH_2), 26.0 (CH_2), 23.5 (CH_2), 23.4(CH_2), 20.4 (CH_3). **ESI-HR-MS** (negative mode) *m/z* calcd. for $[C_{55}H_{90}N_{14}O_{19}\text{-}H]^-$ 1250.65067, found 1250.64236.

Characterisation Data

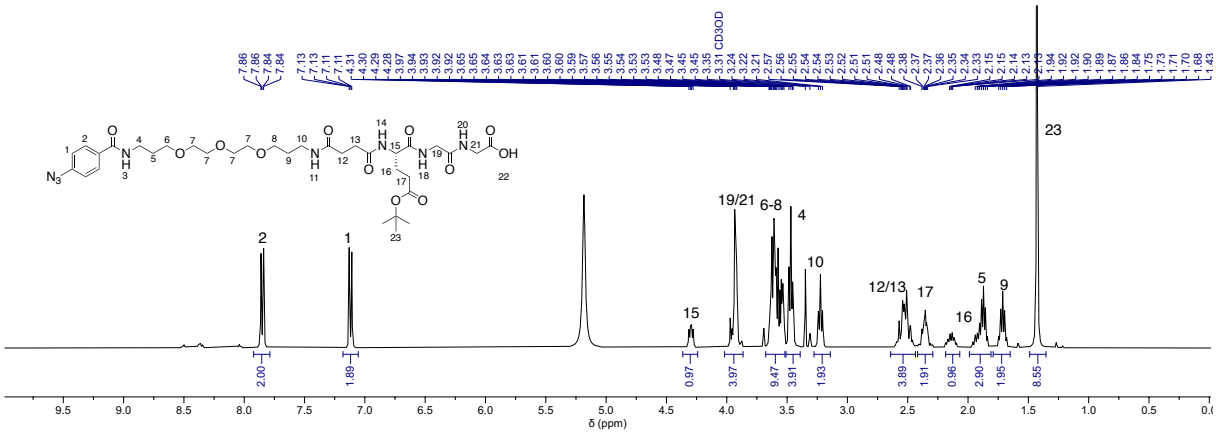

Figure S1. ^{1}H (400 MHz, MeOD, 298 K) NMR spectrum of compound **6a**.

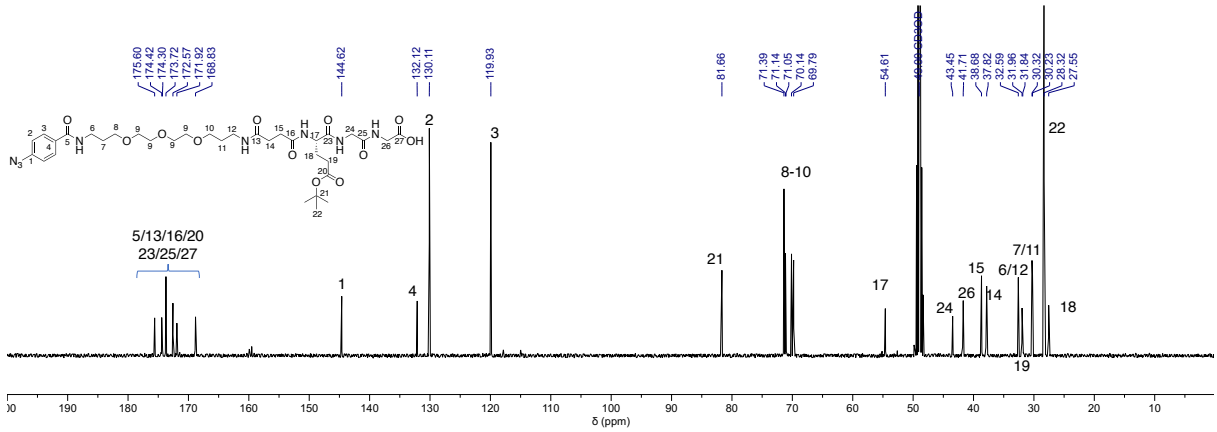

Figure S2. ^{13}C (101 MHz, MeOD, 298 K) NMR spectrum of compound **6a**.

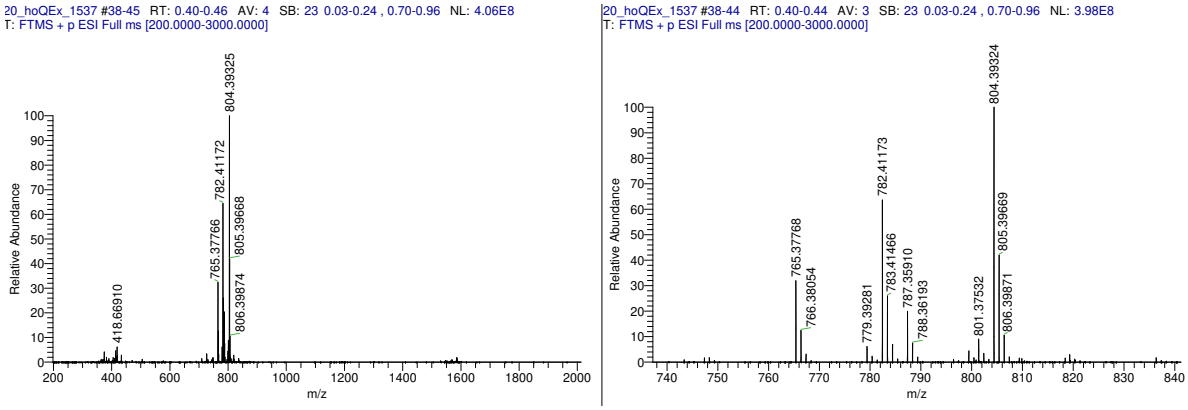

Figure S3. ESI-HR-MS spectrum of compound **6a**.

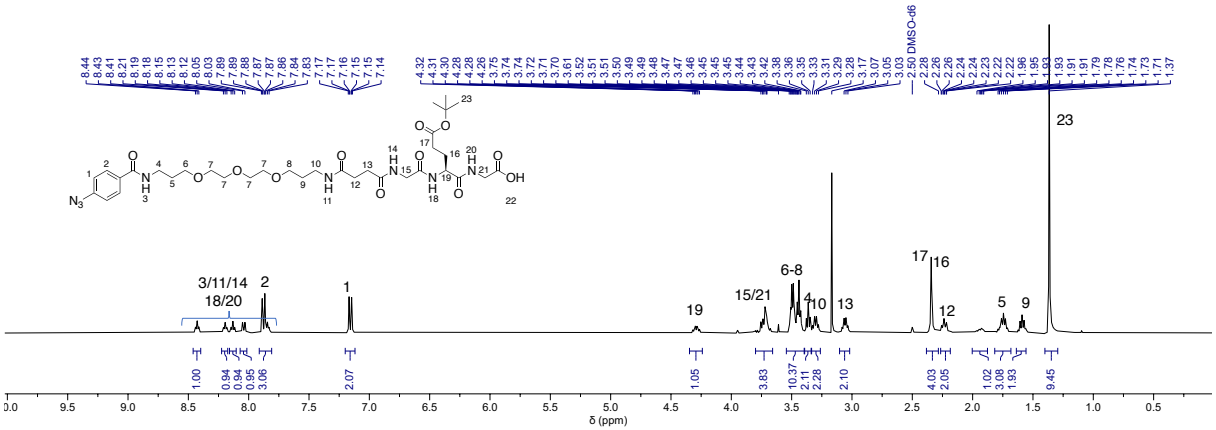

Figure S4. ^{1}H (101 MHz, MeOD, 298 K) NMR spectrum of compound **6b**.

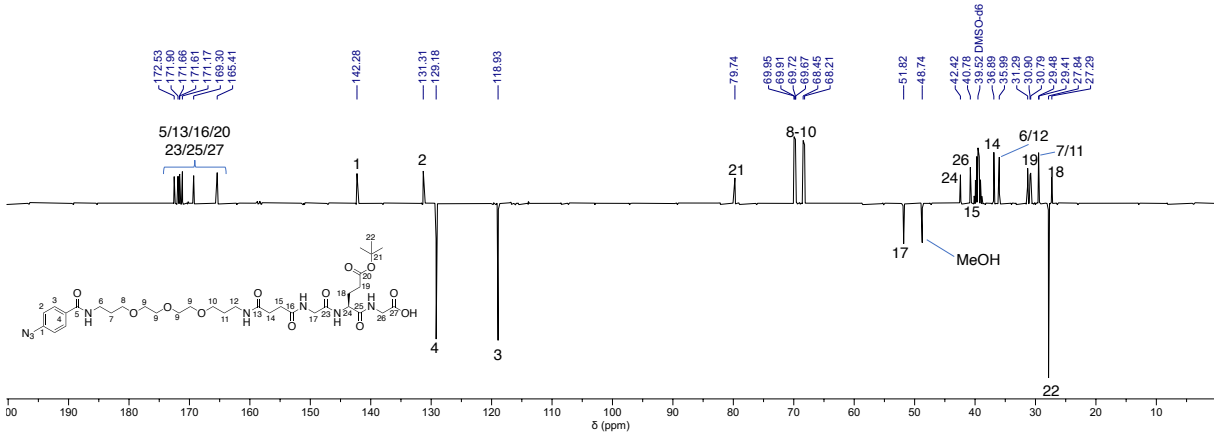

Figure S5. DEPTQ (101 MHz, MeOD, 298 K) NMR spectrum of compound **6b**

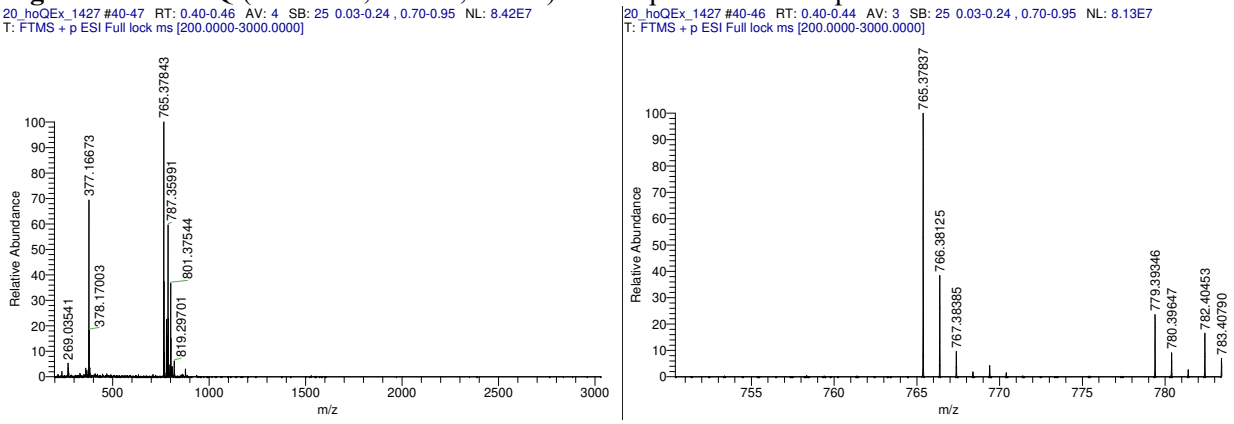

Figure S6. ESI-HR-MS spectrum of compound **6b**.

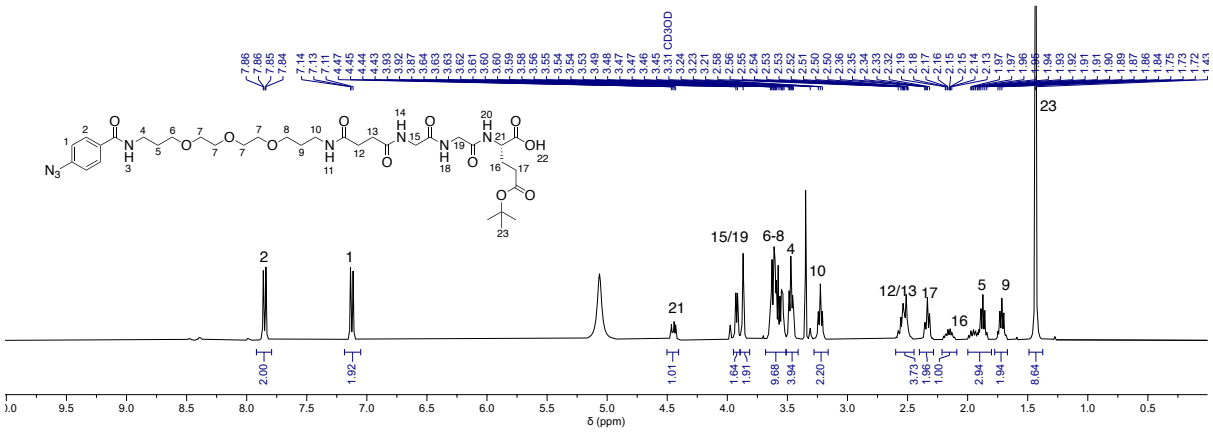

Figure S7. ^{1}H (400 MHz, MeOD, 298 K) NMR spectrum of compound **6c**.

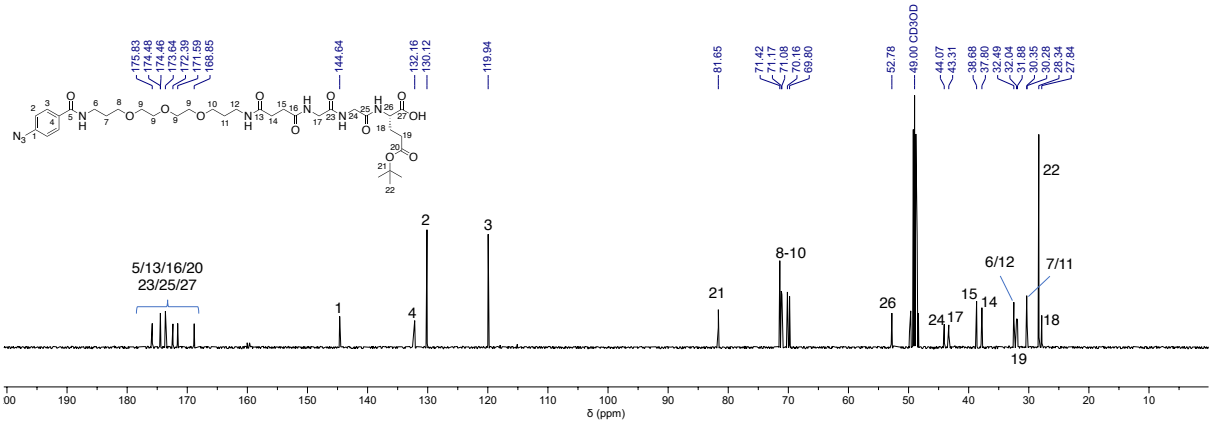

Figure S8. ^{13}C (101 MHz, MeOD, 298 K) NMR spectrum of compound **6c**.

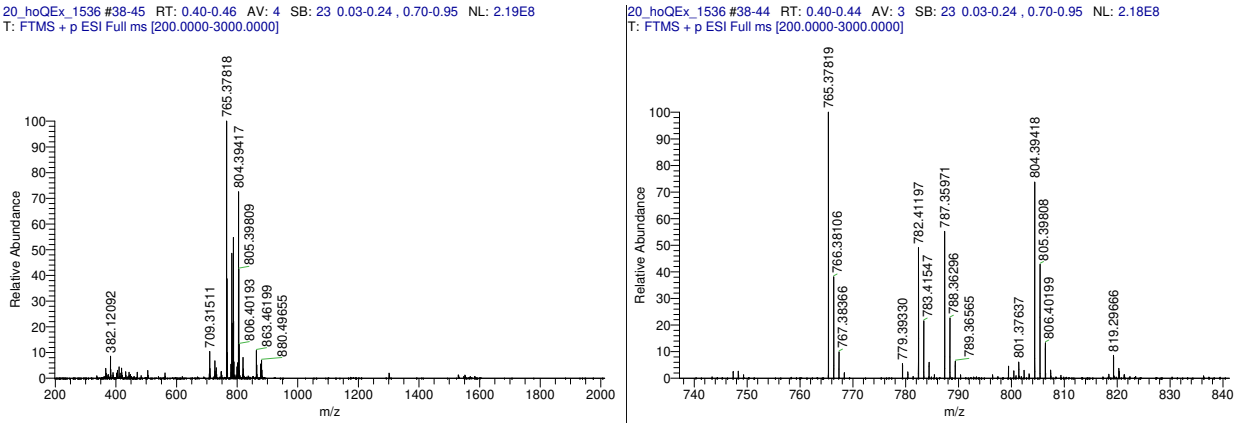

Figure S9. ESI-HR-MS spectrum of compound **6c**.

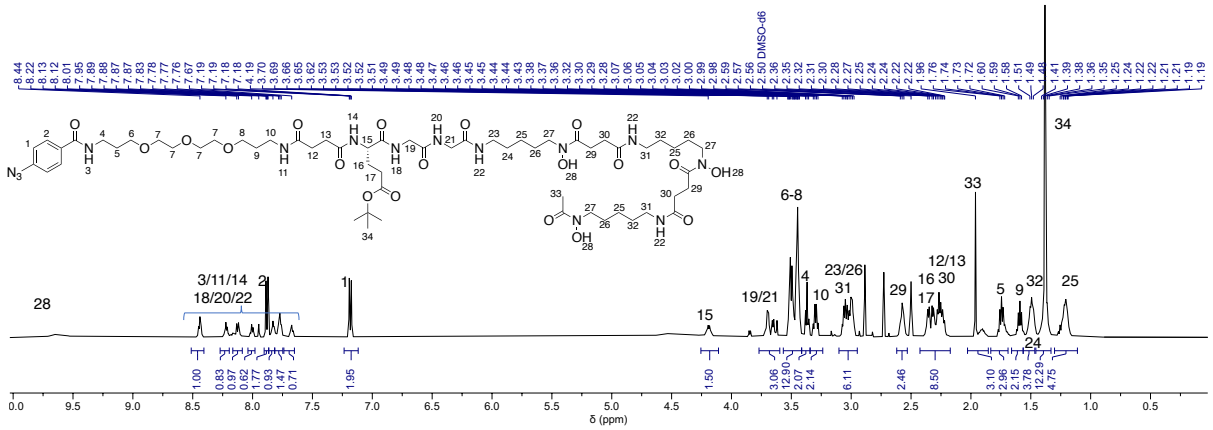

Figure S10. ^{1}H (500 MHz, dmso-d^{6}, 298 K) NMR spectrum of compound **5a**.

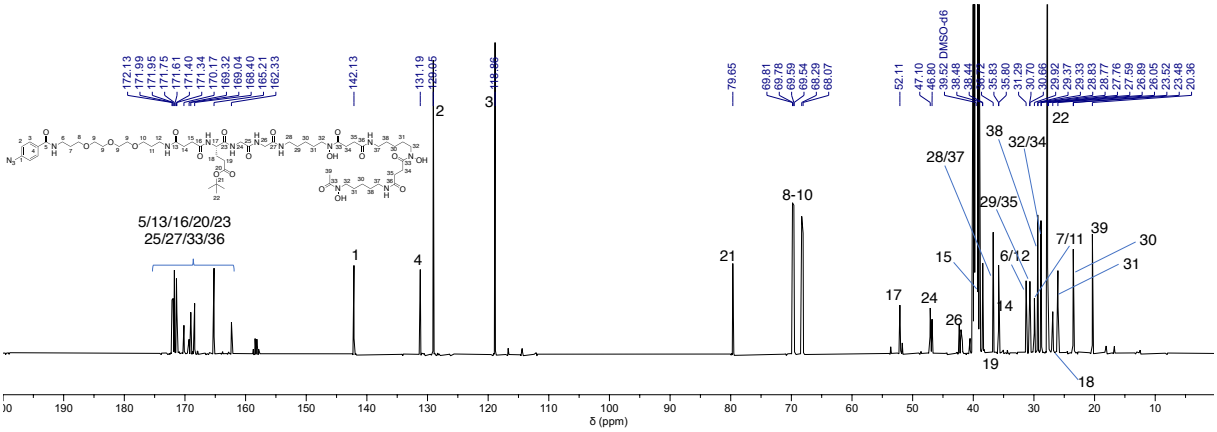

Figure S11. ^{13}C (125 MHz, dmso-d^{6}, 298 K) NMR spectrum of compound **5a**.

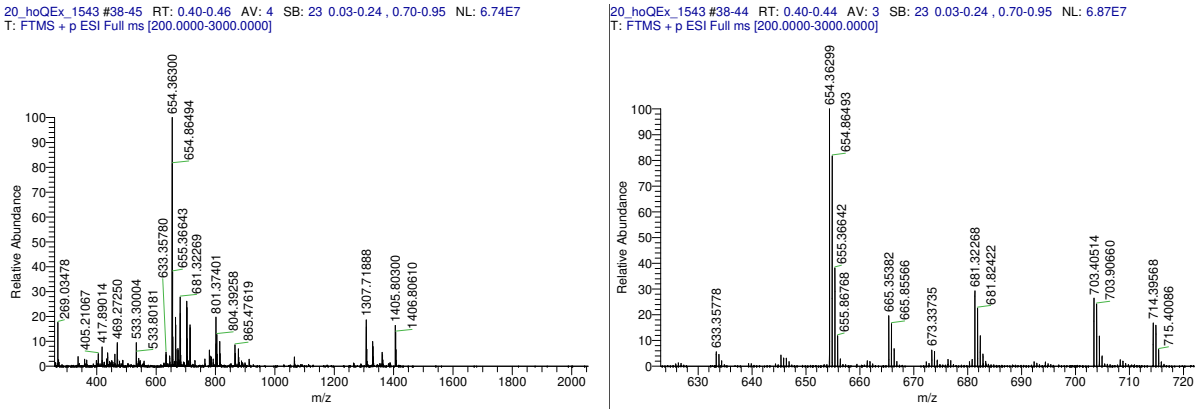

Figure S12. ESI-HR-MS spectrum of compound **5a**.

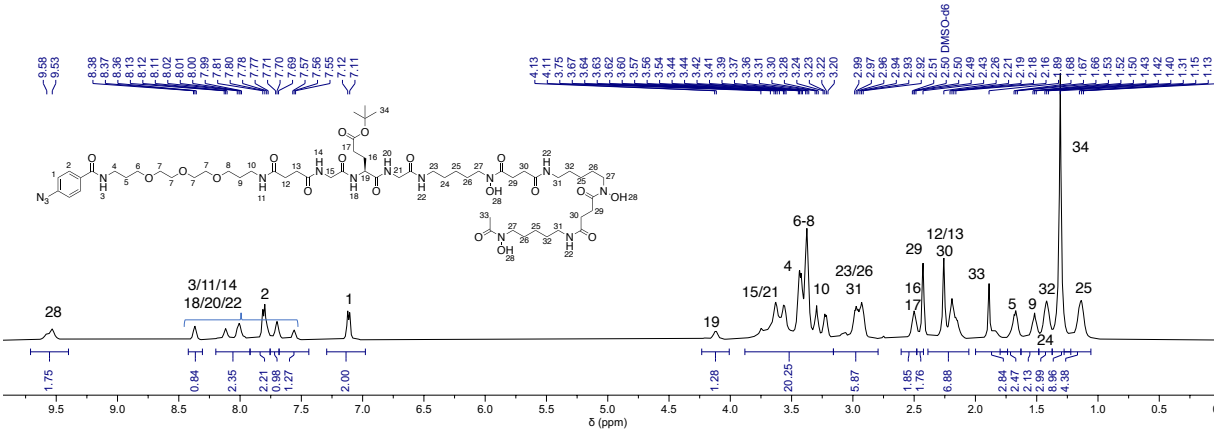

Figure S13. ^{1}H (500 MHz, dmso-d^{6}, 298 K) NMR spectrum of compound **5b**.

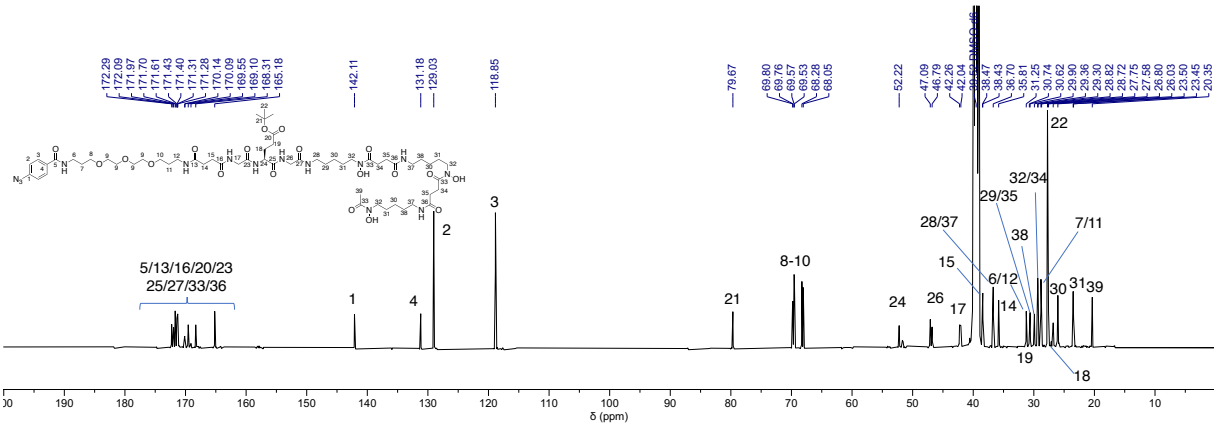

Figure S14. ^{13}C (125 MHz, dmso-d^{6}, 298 K) NMR spectrum of compound **5b**.

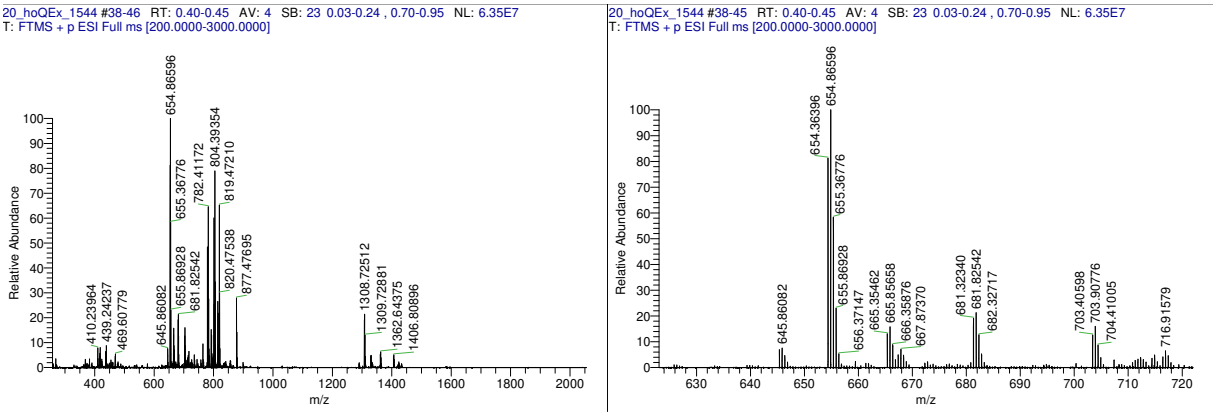

Figure S15. HR-ESI-MS spectrum of spectrum of compound **5b**.

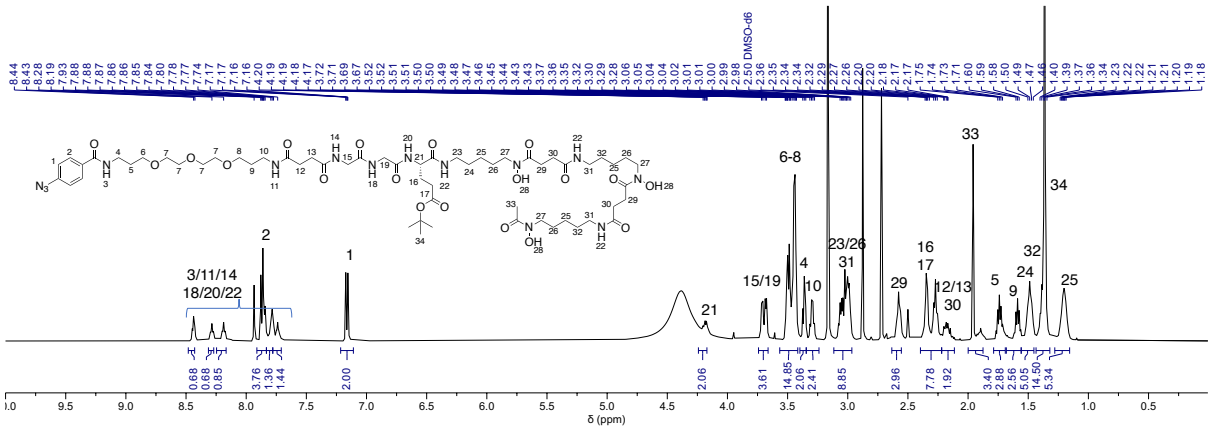

Figure S16. ^{1}H (400 MHz, dmso-d^{6}, 298 K) NMR spectrum of compound **5c**.

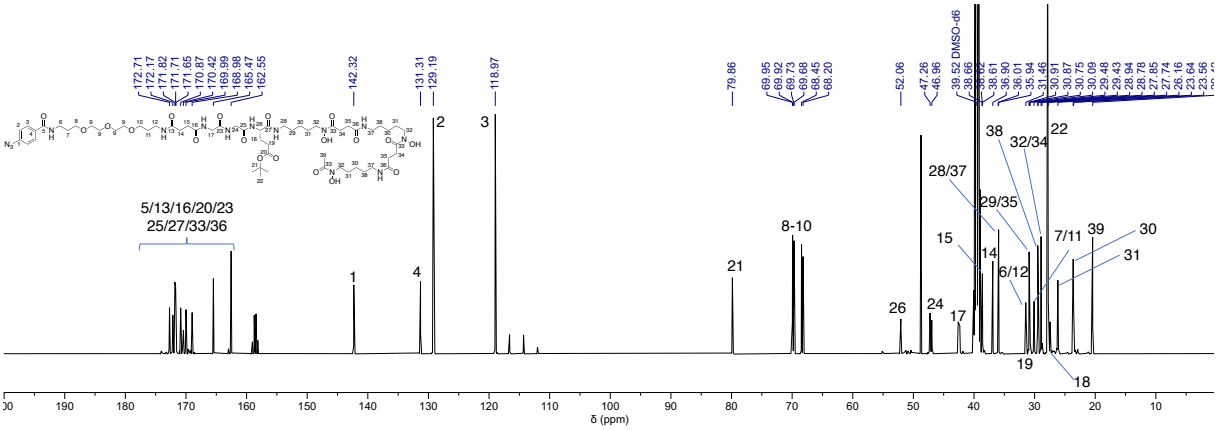

Figure S17. ^{13}C (101 MHz, dmso-d^{6}, 298 K) NMR spectrum of compound **5c**.

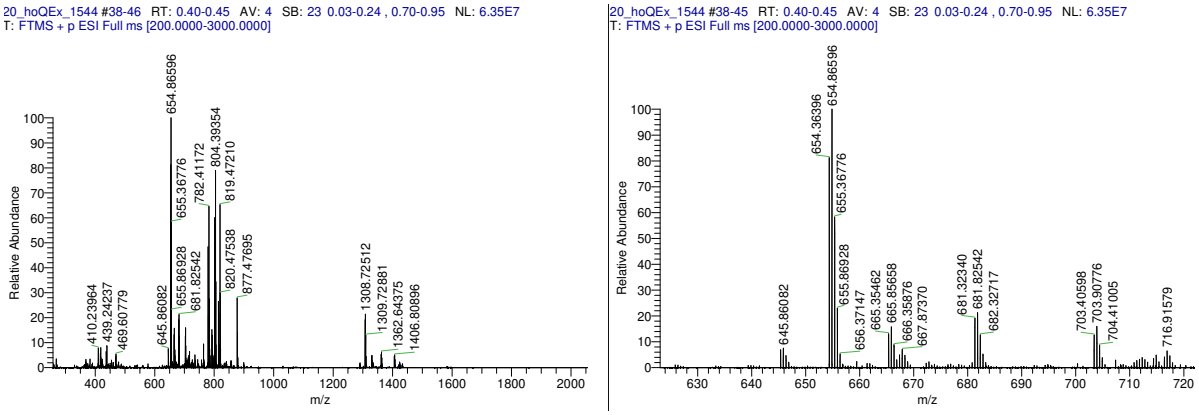

Figure S18. HR-ESI-MS spectrum of spectrum of compound **5c**.

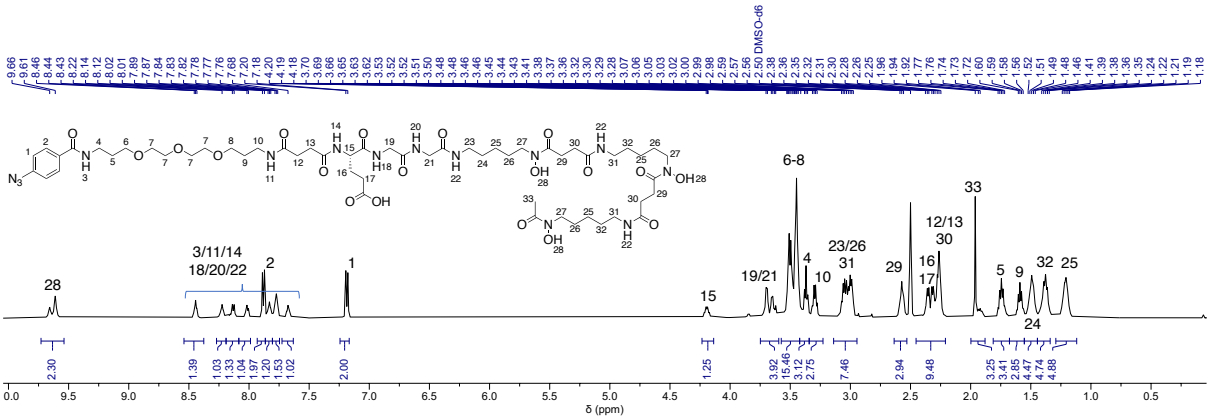

Figure S19. ^{1}H (500 MHz, dmso-d^{6}, 298 K) NMR spectrum of DFO-Gly-Gly-Glu-PEG$_3$-ArN$_3$ (**1**).

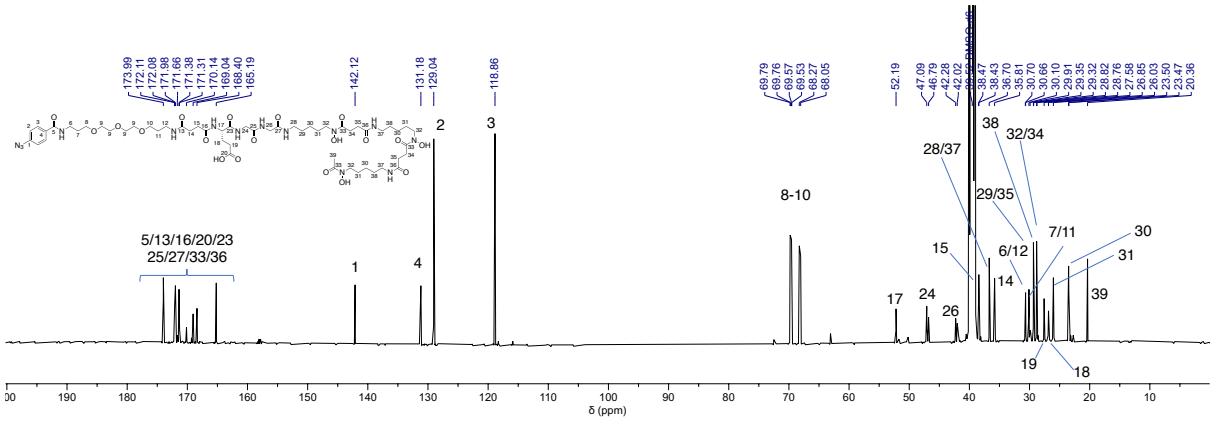

Figure S20. ^{13}C (125 MHz, dmso-d^{6}, 298 K) NMR spectrum of DFO-Gly-Gly-Glu-PEG$_3$-ArN$_3$ (**1**).

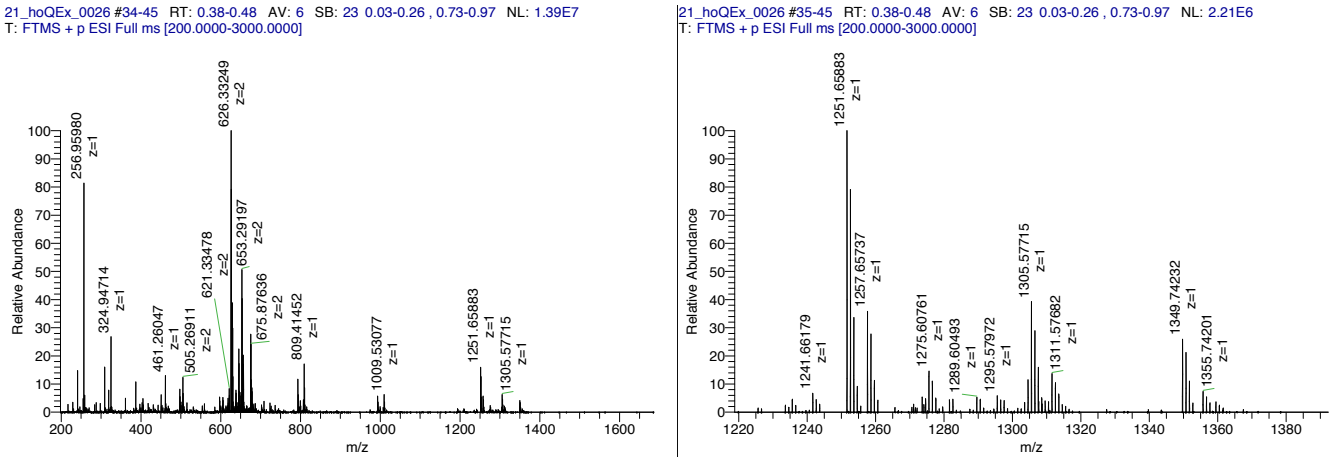

Figure S21. HR-ESI-MS spectrum of spectrum of DFO-Gly-Gly-Glu-PEG$_3$-ArN$_3$ (**1**).

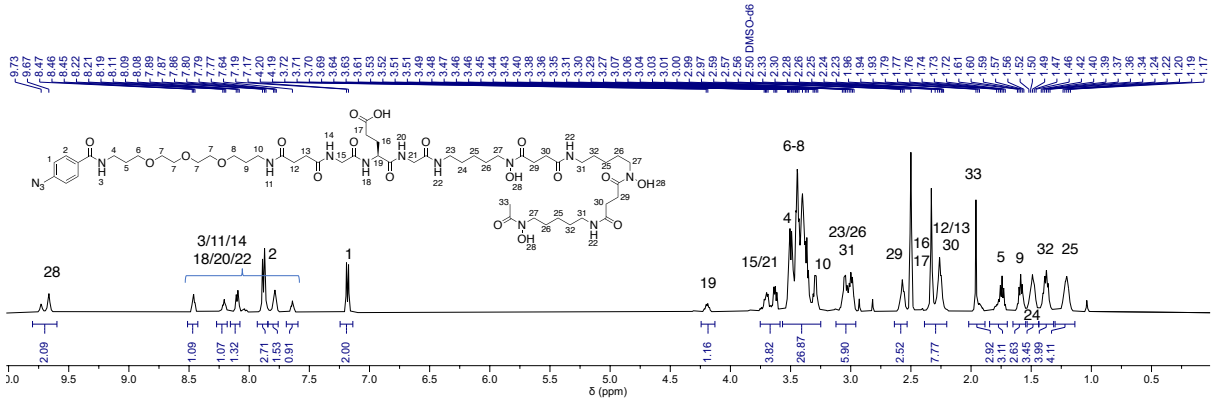

Figure S22. ^{1}H (500 MHz, dmso-d^{6}, 298 K) NMR spectrum of DFO-Gly-Glu-Gly-PEG$_3$-ArN$_3$ (**2**)

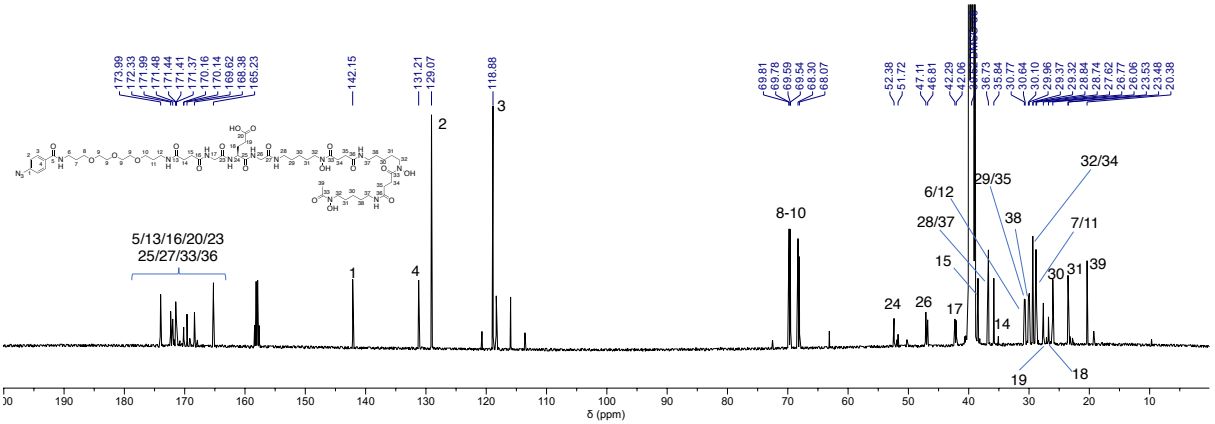

Figure S23. ^{13}C (125 MHz, dmso-d^{6}, 298 K) NMR spectrum of DFO-Gly-Glu-Gly-PEG$_3$-ArN$_3$ (**2**)

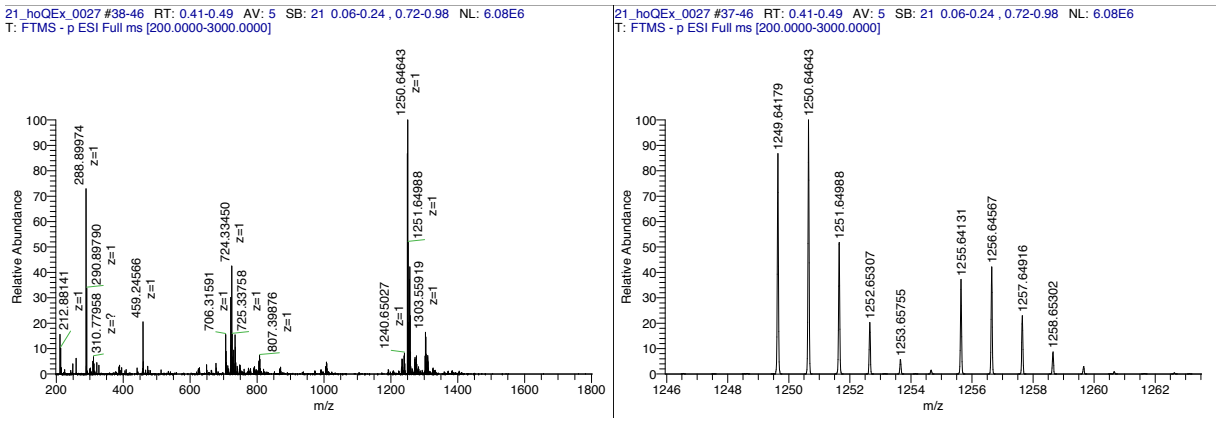

Figure S24. ESI-HR-MS spectrum of DFO-Gly-Glu-Gly-PEG$_3$-ArN$_3$ (**2**).

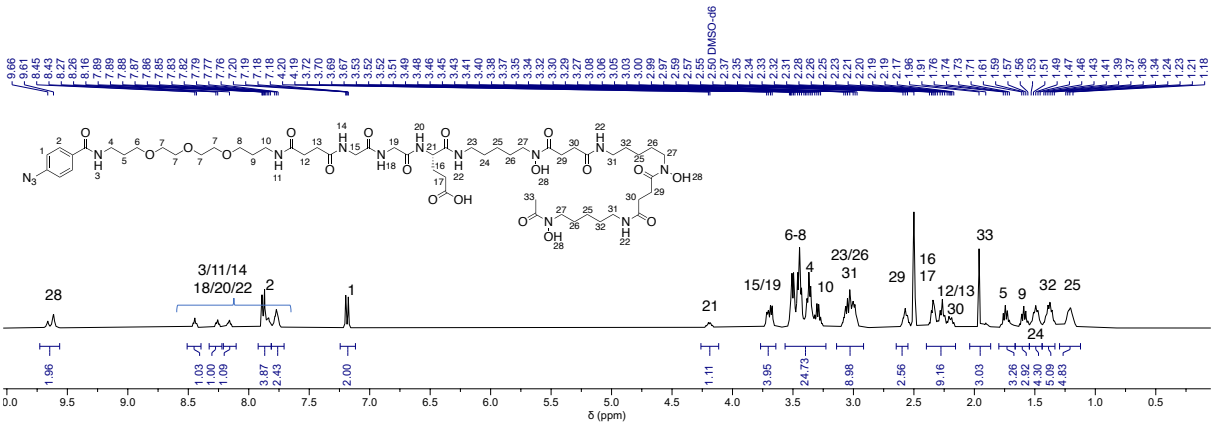

Figure S25. ^{1}H (500 MHz, dmso-d^{6}, 298 K) NMR spectrum of DFO-Glu-Gly-Gly-PEG$_3$-ArN$_3$ (**3**).

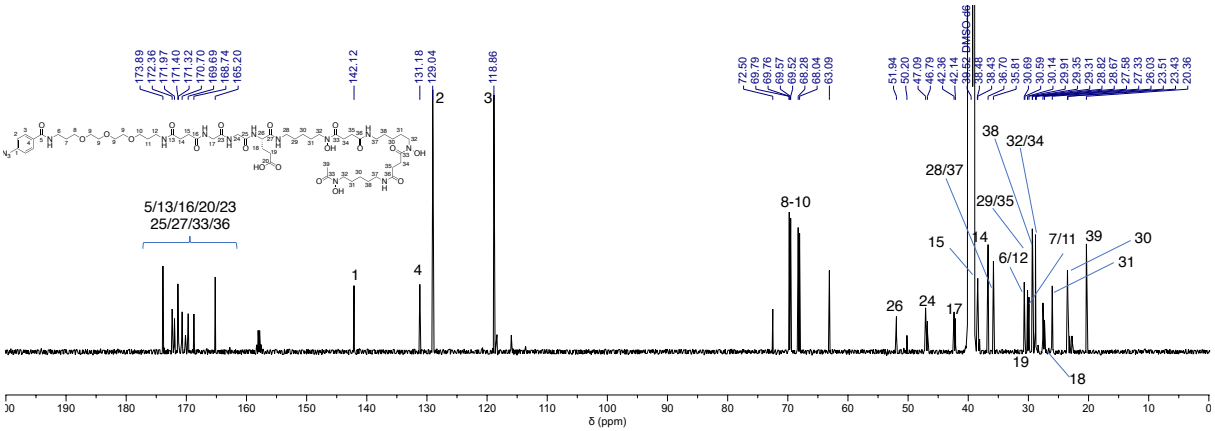

Figure S26. ^{13}C (125 MHz, dmso-d^{6}, 298 K) NMR spectrum of DFO-Glu-Gly-Gly-PEG$_3$-ArN$_3$ (**3**).

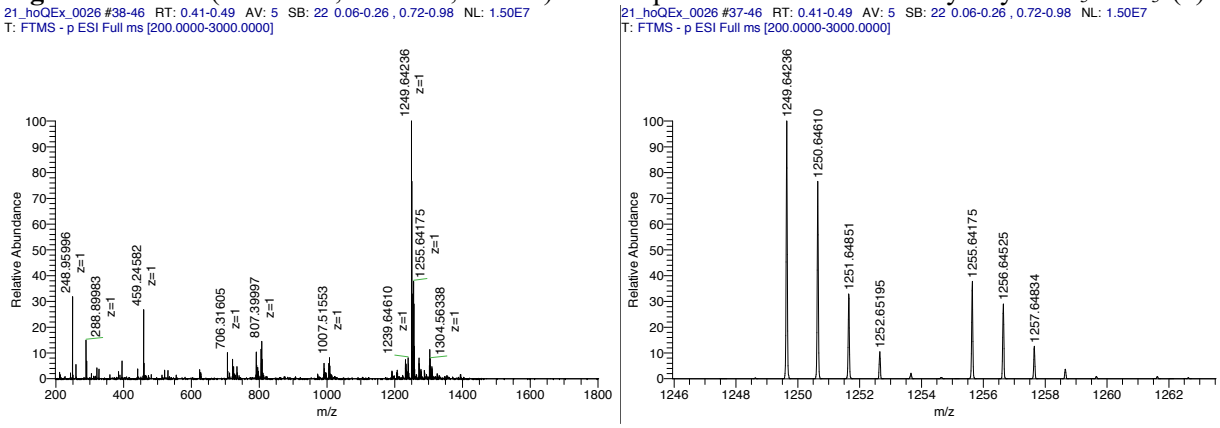

Figure S27. ESI-HR-MS (negative mode) spectrum of DFO-Glu-Gly-Gly-PEG$_3$-ArN$_3$ (**3**).

Zirconium-89 radiolabelling

Radiolabelling reactions to prepare [^{89}Zr]ZrDFO-PEG$_3$-ligands (^{89}Zr-**1** to ^{89}Zr-**4**$^+$) were accomplished by the addition of an aliquot of neutralized [^{89}Zr][Zr(C_2O_4)$_4$]$^{4-}$ stock solution (~6 MBq) to an aqueous solution of DFO-PEG$_3$-ligand (e.g. for **1**, 10 μL of 3.32 mM stock [10% DMSO in H_2O]) with a total reaction volume of 60 μL. The geometry of all reactions was identical. The reactions were monitored by radio-iTLC (50 mM aqueous DTPA at pH 7.0) and complexation was found to be complete in less than 5 min at rt giving a radiochemical conversion (RCC) >99% (R_f = 0.06 – 0.15) for all compounds. The products were characterised by analytical HPLC (Nucleodur EC 250/4, 4 mm ID × 250 mm (C18 HTec, 5 μm) at a flow rate of 1 mL min^{-1} with a linear gradient of A (H_2O containing 0.1% TFA) and B (MeOH containing 0.1% TFA): t = 0 min, 60% A; t = 11 min, 5% A.

Stability studies in vitro

Human Serum challenge. For each experiments ~2 MBq (20 μL, 11 nmol) of ^{89}Zr-**1** to ^{89}Zr-**4**$^+$ were mixed in 150 μL of Human serum. The samples were incubated at 37°C for 72h. The dissociation of the radiocomplexes was monitored by radio-iTLC (50 mM aqueous DTPA at pH 7.0). Experiments were performed in triplicate.

H_4EDTA stability measurements. For each experiments ~2 MBq (20 μL, 11 nmol) of ^{89}Zr-**1** to ^{89}Zr-**4**$^+$ were diluted in PBS 1X (110 μL, pH 7.4) and a solution of H_4EDTA (20 μL, 11 μmol). The pH of the solutions was adjusted to pH 7.4 using aliquots of 0.1M $NaHCO_3$ when needed. The samples were incubated at rt for 72h. The dissociation of the radiocomplexes was monitored by radio-iTLC (50 mM aqueous DTPA at pH 7.0). Experiments were performed in triplicate.

$^{nat}Fe^{3+}$ exchange experiments. For each experiments ~2 MBq (20 μL, 11 nmol) of ^{89}Zr-**1** to ^{89}Zr-**4**$^+$ were diluted in PBS 1X (128 μL, pH 7.4) and an aqueous solution of $FeCl_3$ (2 μL, 11 nmol). The pH of the solutions was adjusted to pH 7.4 using aliquots of 0.1M $NaHCO_3$ when needed. The samples were incubated at rt for 72h. The dissociation of the radiocomplexes was monitored by radio-iTLC (50 mM aqueous DTPA at pH 7.0). Experiments were performed in triplicate.

^{89}Zr-photoradiolabelling of MetMAb^{TM}

MetMAb^{TM} (60 mg mL^{-1}, 35 μL, 21.2 nmol of onartuzumab protein, MW 99.16 kDa) in formulation buffer (10 nmol L^{-1} histidine succinate, 106 nmol L^{-1} trehalose dihydrate, 0.02% polysorbate 20, pH 5.7) was incubated with DFO-Gly-Glu-Gly-PEG$_3$-ArN$_3$ (**2**) (2.32 mM, 10 μL, 23.3 nmol) in Chelex-treated water (80 μL) at pH 8 – 8.4 and ^{89}Zr(oxalate) (10 MBq, 20 μL). Reactions were irradiated at 100% LED intensity (395 nm) for 15 min. After the irradiation, aliquots of the crude reaction mixtures were purified by preparative PD-10-SEC (collecting the 0.0 – 1.6 mL high molecular weight fraction using sterile PBS as an eluent). Crude and purified aliquots were analysed by using analytical radio-iTLC, PD-10-SEC and SEC-HPLC.

Table S1. *Percentage of the intact radiocomplexes observed in stability studies in with human serum, EDTA and Fe(III) after 72 h.*

	^{89}Zr-**1**	^{89}Zr-**2**	^{89}Zr-**3**	^{89}Zr-**4**$^{+}$
Human serum	91.3 ± 1.88	92.8 ± 1.66	93.7 ± 2.54	95.4 ± 1.34
EDTA	36.2 ± 15.4	94.9 ± 1.74	93.5 ± 3.18	93.8 ± 2.07
Fe(III)	90.8 ± 4.31	87.9 ± 4.98	87.5 ± 5.76	88.8 ± 5.03

Small-animal PET imaging with [^{89}Zr]ZrDFO-2-onartuzumab

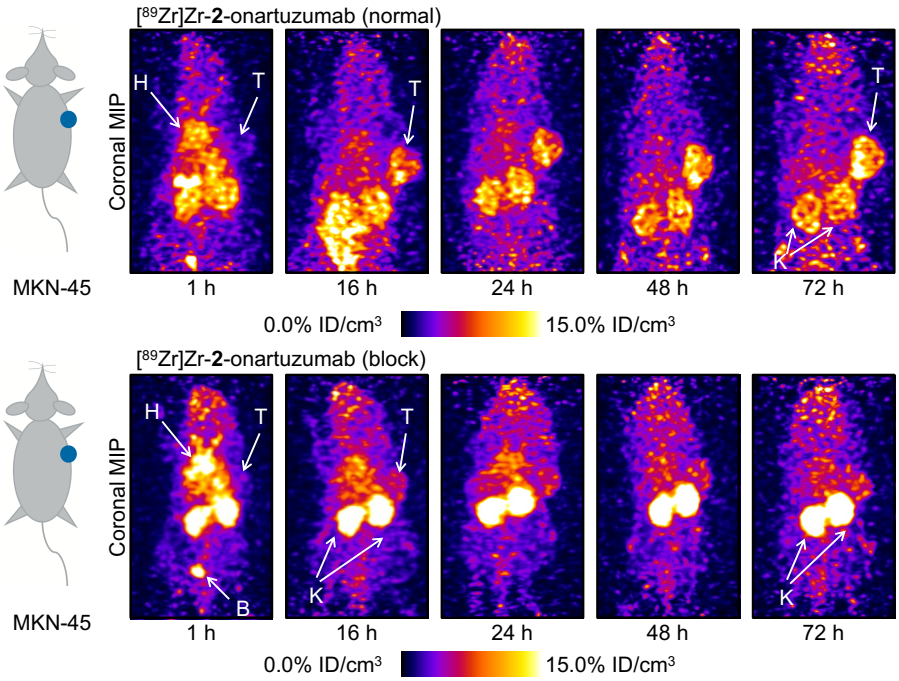

Figure S28. Maximum intensity projection (MIP) PET images recorded in athymic nude mice bearing MKN-45 tumours on the right flank at time points between 1 h to 72 h post-administration of the radiotracers for (top) [^{89}Zr]Zr-**2**-onartuzumab (normal group), and (bottom) [^{89}Zr]Zr-**2**-onartuzumab (blocking group). T = tumour, H = heart, L = liver, B = bladder, K = Kidneys.

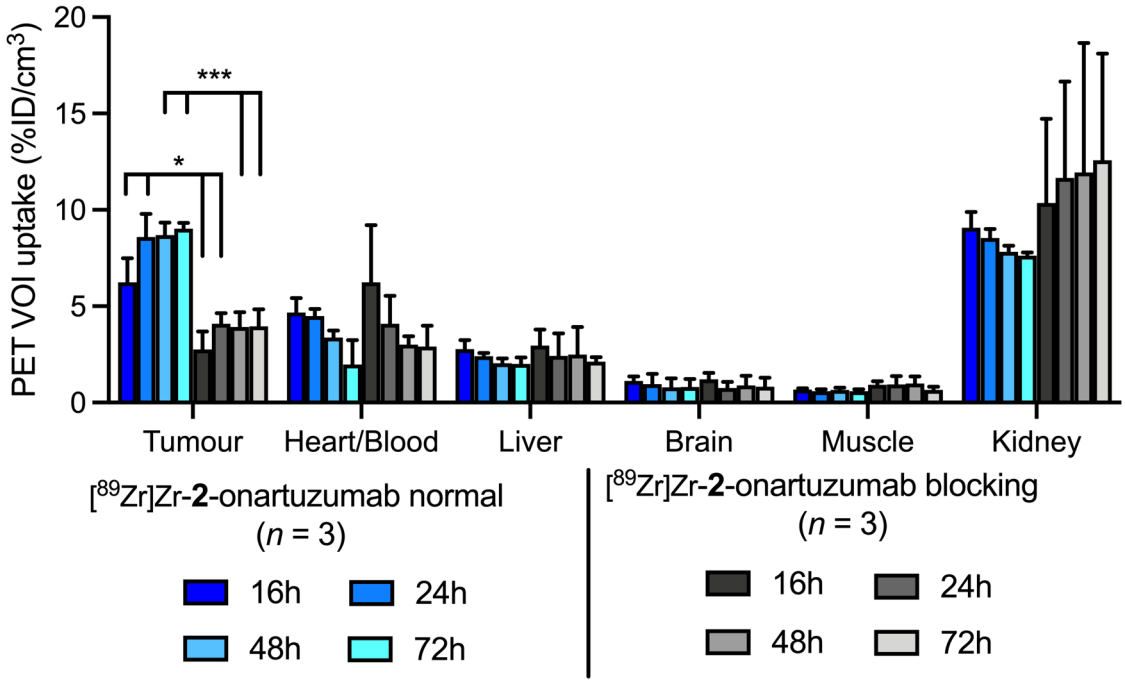

Figure S29. VOI analysis from PET imaging at 16, 24, 48 and 72 h for uptake of [^{89}Zr]Zr-**2**-onartuzumab in the normal and blocking groups. Data are displayed as %ID/cm^3.

Measured effective half-lives

The effective half-life $t_{1/2}$(eff) of [^{89}Zr]Zr-**2**-onartuzumab was measured in the MKN-45 tumour model group in the same athymic nude mice used for small-animal PET imaging and biodistribution studies. Total internal radioactivity was measured as a function of time by using a dose calibrator.

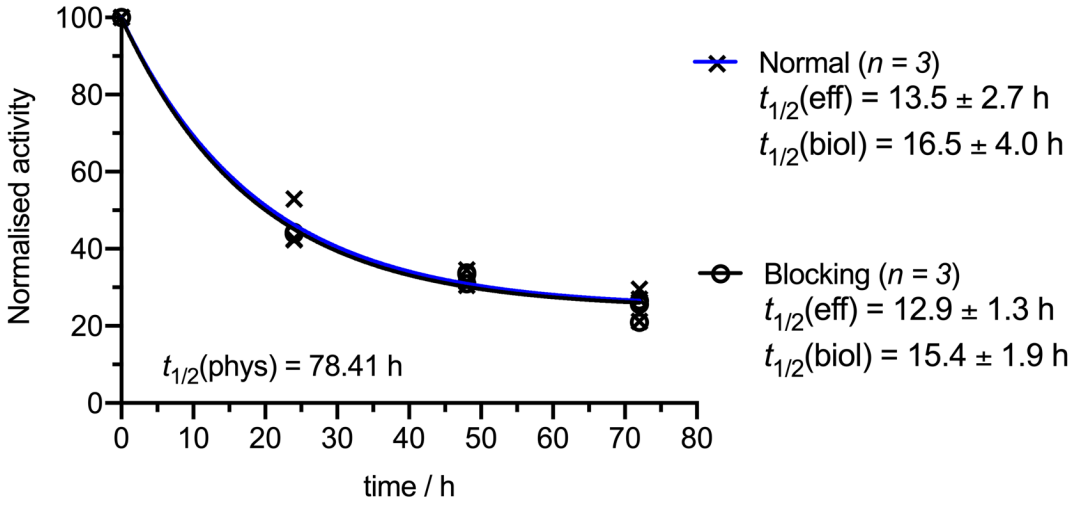

Figure S30. Plot of the measure activity retained in the normal (black) and blocking (blue) groups *versus* time after admistration of [^{89}Zr]Zr-**2**-onartuzumab in MKN-45 tumour bearing mice.

Biodistribution results

Table S2. *Ex vivo* biodistribution data measured at 72 h after i.v. administration of [^{89}Zr]Zr-**2**-onartuzumab (normal and blocking groups) in female athymic nude mice bearing subcutaneous MKN-45 tumours.

	[^{89}Zr]Zr-**2**-onartuzumab (normal group, n = 3)		[^{89}Zr]Zr-**2**-onartuzumab (blocking group, n = 3)	
Tissue	Uptake / %ID g^{-1} ± S.D.[a]	Tumour-to-tissue contrast ratio ± S.D.[b]	Uptake / %ID g^{-1} ± S.D.[a]	Tumour-to-tissue contrast ratio ± S.D.[b]
Blood	2.70 ± 0.30	2.85 ± 0.55	6.44 ± 3.34	0.65 ± 0.35
Tumour	7.69 ± 1.23	1.00 ± 0.00	4.18 ± 0.64	1.00 ± 0.22
Heart	1.22 ± 0.40	6.30 ± 2.30	1.53 ± 0.72	2.73 ± 1.35
Lungs	1.58 ± 0.21	4.85 ± 1.01	2.26 ± 0.62	1.85 ± 0.58
Liver	2.10 ± 0.45	3.66 ± 0.98	2.07 ± 0.76	2.02 ± 0.81
Spleen	1.00 ± 0.31	7.73 ± 2.68	1.77 ± 0.50	2.36 ± 0.75
Stomach	0.36 ± 0.03	21.28 ± 3.95	0.34 ± 0.18	12.37 ± 6.77
Pancreas	0.47 ± 0.07	16.52 ± 3.69	0.55 ± 0.14	7.54 ± 2.23
Kidney	12.01 ± 0.81	0.64 ± 0.11	26.98 ± 15.64	0.15 ± 0.09
Sm. Int.	0.39 ± 0.15	19.66 ± 8.08	0.48 ± 0.24	8.71 ± 4.55
Large Int.	0.37 ± 0.13	20.94 ± 8.39	0.59 ± 0.39	7.11 ± 4.84
Muscle	0.43 ± 0.21	17.69 ± 5.49	0.56 ± 0.22	7.41 ± 3.09
Bone	1.01 ± 0.34	7.60 ± 2.83	1.80 ± 0.53	2.33 ± 0.78
Skin	1.87 ± 0.61	4.10 ± 1.48	2.30 ± 1.24	1.82 ± 1.01

[a] Uptake data are expressed as the mean %ID g^{-1} ± one standard deviation (S.D.). [b] Errors for the tumour-to-tissue ratios are calculated as the standard deviations based on ratios from dependent pairs.

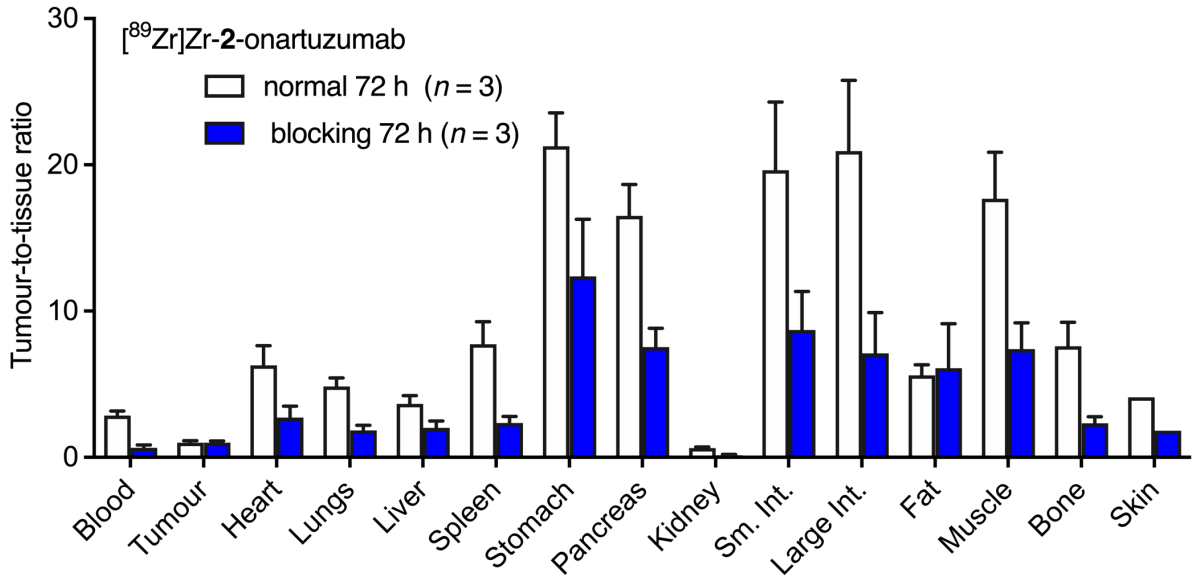

Figure S31. Tumour-to-tissue contrast ratios from the biodistribution of [^{89}Zr]Zr-**2**-onartuzumab in mice bearing subcutaneous MKN-45 tumours.

References

1. Zanzonico P. Routine Quality Control of Clinical Nuclear Medicine Instrumentation: A Brief Review. *J Nucl Med*. 2008;49:1114-1131.
2. Sert, N. P. du; Ahluwalia, A.; Alam, S.; Avey, M. T.; Baker, M.; Browne, W. J.; Clark, A.; Cuthill, I. C.; Dirnagl, U.; Emerson, M.; Garner, P.; Holgate, S. T.; Howells, D. W.; Hurst, V.; Karp, N. A.; Lazic, S. E.; Lidster, K.; MacCallum, C. J.; Macleod, M.; Pearl, E. J.; Petersen, O. H.; Rawle, F.; Reynolds, P.; Rooney, K.; Sena, E. S.; Silberberg, S. D.; Steckler, T.; Würbel, H. Reporting Animal Research: Explanation and Elaboration for the ARRIVE Guidelines 2.0. *PLOS Biology* **2020**, *18* (7), e3000411. https://doi.org/10.1371/journal.pbio.3000411.
3. Fridman R, Benton G, Aranoutova I, Kleinman HK, Bonfil RD. Increased initiation and growth of tumor cell lines, cancer stem cells and biopsy material in mice using basement membrane matrix protein (Cultrex or Matrigel) co-injection. *Nat Protoc*. 2012;7:1138-1144.
4. Bai B, Dahlbom M, Park R, et al. Performance comparison of GENISYS4 and microPET preclinical PET scanners. *IEEE Nucl Sci Symp Conf Rec*. 2012;bai:3765-3768.
5. Frisch, M. J.; Trucks, G. W.; Schlegel, H. B.; Scuseria, G. E.; Robb, M. A.; Cheeseman, J. R.; Scalmani, G.; Barone, V.; Mennucci, B.; Petersson, G. A.; Nakatsuji, H.; Caricato, M.; Li, X.; Hratchian, H. P.; Izmaylov, A. F.; Bloino, J.; Zheng, G.; Sonnenberg, J. L.; Hada, M.; Ehara, M.; Toyota, K.; Fukuda, R.; Hasegawa, J.; Ishida, M.; Nakajima, T.; Honda, Y.; Kitao, O.; Nakai, H.; Vreven, T.; Montgomery Jr., J. A.; Peralta, J. E.; Ogliaro, F.; Bearpark, M.; Heyd, J. J.; Brothers, E.; Kudin, K. N.; Staroverov, V. N.; Kobayashi, R.; Normand, J.; Raghavachari, K.; Rendell, A.; Burant, J. C.; Iyengar, S. S.; Tomasi, J.; Cossi, M.; Rega, N.; Millam, J. M.; Klene, M.; Knox, J. E.; Cross, J. B.; Bakken, V.; Adamo, C.; Jaramillo, J.; Gomperts, R.; Stratmann, R. E.; Yazyev, O.; Austin, A. J.; Cammi, R.; Pomelli, C.; Ochterski, J. W.; Martin, R. L.; Morokuma, K.; Zakrzewski, V. G.; Voth, G. A.; Salvador, P.; Dannenberg, J. J.; Dapprich, S.; Daniels, A. D.; Farkas, □.; Foresman, J. B.; Ortiz, J. V; Cioslowski, J.; Fox, D. J. Gaussian16 (Revision A.03), Gaussian Inc. Wallingford CT. *Gaussian16 (Revision A.03)*. 2016.
6. Chen, J. L.; Noodleman, L.; Case, D. A.; Bashford, D. Incorporating Solvation Effects into Density Functional Electronic Structure Calculations. *J. Phys. Chem.* **1994**, *98* (43), 11059–11068. https://doi.org/10.1021/j100094a013.

7. Lee, C.; Yang, W.; Parr, R. G. Development of the Colle-Salvetti Correlation-Energy Formula into a Functional of the Electron Density. *Phys. Rev. B* **1988**, *37* (2), 785–789. https://doi.org/10.1103/PhysRevB.37.785.
8. Becke, A. D. Density-Functional Exchange-Energy Approximation with Correct Asymptotic Behavior. *Phys. Rev. A* **1988**, *38* (6), 3098–3100. https://doi.org/10.1103/PhysRevA.38.3098.
9. Stephens, P. J.; Devlin, F. J.; Chabalowski, C. F.; Frisch, M. J. Ab Initio Calculation of Vibrational Absorption and Circular Dichroism Spectra Using Density Functional Force Fields. *J. Phys. Chem.* **1994**, *98* (45), 11623–11627. https://doi.org/10.1021/j100096a001.
10. Godbout, N.; Salahub, D. R.; Andzelm, J.; Wimmer, E. Optimization of Gaussian-Type Basis Sets for Local Spin Density Functional Calculations. Part I. Boron through Neon, Optimization Technique and Validation. *Can. J. Chem.* **1992**, *70* (2), 560–571. https://doi.org/10.1139/v92-079.
11. Sosa, C.; Andzelm, J.; Elkin, B. C.; Wimmer, E.; Dobbs, K. D.; Dixon, D. A. A Local Density Functional Study of the Structure and Vibrational Frequencies of Molecular Transition-Metal Compounds. *J. Phys. Chem.* **1992**, *96* (16), 6630–6636. https://doi.org/10.1021/j100195a022.